International Journal of Multiphase Flow 35 (2009) 1017–1035

Contents lists available at ScienceDirect

International Journal of Multiphase Flow

journal homepage: www.elsevier.com/locate/ijmulflow

Suspensions in turbulent liquid pipe flow: Kinetic modelling and added mass effects

R. Skartlien [a,*], D. Drazen [b], D.C. Swailes [c], A. Jensen [b]

[a] Institute for Energy Technology, P.O. Box 40, N-2027 Kjeller, Norway
[b] University of Oslo, Department of Mathematics, Mechanics Division, P.O. Box 1053 Blindern, N-0316 Oslo, Norway
[c] School of Mechanical and Systems Engineering, Stephenson Building, Claremont Road, Newcastle University, Newcastle upon Tyne NE1 7RU, United Kingdom

ARTICLE INFO

Article history:
Received 6 January 2009
Received in revised form 2 June 2009
Accepted 5 July 2009
Available online 8 July 2009

Keywords:
Turbulent suspensions
Particle diffusivity
Virtual mass
Added mass
Particle continuum equations
Kinetic theory

ABSTRACT

We develop a Eulerian model for a particle suspension in fully developed turbulent liquid in a horizontal pipe. Virtual mass effects and hydrodynamic interactions are accounted for by an extension of the kinetic theory of Reeks and Swailes.

The model input is provided by the fluid–turbulence statistics measured using PIV. The model output is compared to PTV data in terms of concentration and particle kinetic stresses. We use water as carrier fluid, and polystyrene particles of diameter 950 μm. The flow Reynolds numbers are 43,000, 64,000 and 115,000, with corresponding particle Stokes numbers (in terms of the turbulence timescale seen by the particles) of 1.3, 2.5 and 3.0.

We find that the radial component of the particle kinetic stress controls the radial diffusivity and the scale height of the concentration profile. It is shown that the axial and radial normal stresses are larger than the corresponding fluid stresses, mainly due to the virtual mass force. A model for hydrodynamic (long-range) interaction between the particles is invoked to account for the radial normal stress profile. As has been found previously in gas–solid flow, this interaction serves to redistribute the axial normal stress to the radial normal stress. The transport of kinetic stress is insignificant, leading to local relations between particle and fluid stresses, and a local particle diffusivity. The axial normal stress induced by the mean velocity shear is small compared to the virtual mass contribution.

1. Introduction

1.1. Background

The transport of fluid droplets, bubbles or solid particles in a turbulent carrier fluid is a challenging topic in multiphase pipe flow. Three common subgroups of such flows are droplets suspended in gas, droplets suspended in another fluid (dispersions) and solid particles suspended in a liquid (suspensions). Two major challenges in the accompanying modelling effort are to predict the distribution of the dispersed phase in inhomogeneous turbulence, and how the carrier fluid turbulence is affected. A central issue in the modelling effort is how to treat the boundary conditions. These depend on the specific problem at hand, e.g., entrainment of droplets into the carrier fluid or particle–particle/wall–particle interactions.

In an accompanying paper, Skartlien (2009) addresses the modelling of droplets in a dense gas flow representative of conditions in pipelines. In the current paper, we discuss the modelling of solid particles suspended in a turbulent liquid. This setting is chosen to enable a more fundamental experimental and theoretical study of carrier fluid turbulence and the effect on particle dynamics. Furthermore, some of the experimental difficulties associated with turbulence measurements in droplet laden gas–liquid pipe flow at high Reynolds numbers are then circumvented. These difficulties should however decrease for lower bulk velocity. In the droplet model of Skartlien (2009), the particle kinetic theory developed at the University of Newcastle by Reeks (1992, 1993), Swailes et al. (1998) was adopted.

In the current work, we extend this theory to account for the added mass effect that occurs for solid particles (also for bubbles and fluid droplets) suspended in a liquid, provided that the particle/carrier fluid material density ratio is of order unity or smaller. This is the first time the added mass effect has been addressed in the context of pdf equations and the associated closure laws in the accompanying continuum equations.

The added mass effect introduces additional hydrodynamic forcing on the particles and is a source of extra dispersion/turbulent diffusion with larger effects for smaller material density ratio. The current experimental campaign has enabled us to test the model ingredients and assumptions, and the subsequent turbulence data have provided the required input to the model. Drazen and Jensen (in preparation) present the current experimental work in more detail. The data were obtained by a combination of Particle Image Velocimetry (PIV) and Tracking Velocimetry (PTV), using a

* Corresponding author. Tel.: +47 63 80 64 67; fax: +47 63 81 11 68.
E-mail address: roar.skartlien@ife.no (R. Skartlien).

0301-9322/$ - see front matter © 2009 Elsevier Ltd. All rights reserved.
doi:10.1016/j.ijmultiphaseflow.2009.07.001

high-speed digital camera and a dual pulsed laser to enable simultaneous measurements of the carrier fluid velocity and particle motions. We will give a brief overview of the experiments below.

Recent experimental work in the literature has focused on turbulence modification. Kiger and Pan (2000) used glass beads (with diameter 195 μm) suspended in turbulent channel flow with water. Wu et al. (2006) used polythene spheres with diameter 60 and 110 μm, in air flow. Both authors found turbulence augmentation even at low mass loadings less than or equal to 10^{-3}. In the current dataset, Drazen and Jensen (2007, in preparation) found significant turbulence enhancement ($\sim 20\%$) of the carrier fluid with polystyrene particles in water at a volume fraction of $\sim 10^{-3}$. Gore and Crowe (1989) discuss the effect of particle size on turbulence modulation, while Hetsroni (1989) discusses the dependency on particle Reynolds number. A general trend is that larger particles and particle Reynolds numbers tend to augment turbulence, while smaller particles tend to suppress turbulence. More theoretical studies that attempt to explain the modulation phenomenon in more detail can be found in Kenning and Crowe (1997), Crowe (2000) and Poelma and Ooms (2006). Many authors have also used DNS to analyze turbulence modulation (e.g., Ahmed and Elghobashi, 2000; Ferrante and Elghobashi, 2003). We will also focus on the modelling of turbulence modification in an upcoming paper, using the current dataset.

In this paper, we will not focus on the modification of turbulence, but consider the measured turbulence profiles as given input to the suspension model. The novelty of the current work is in the combination of PIV/PTV data with the kinetic model, accounting for both the added mass and drag-force. We adopt the kinetic theory of Reeks (1992, 1993), Swailes et al. (1998), Hyland et al. (1999) for a particle suspension in turbulent fluid. Recent developments can be found in Reeks (2005), in particular with respect to the requirement of a "well mixed" homogeneous distribution of passive tracer particles in incompressible carrier fluid. This kinetic approach provides the Eulerian mass, momentum and kinetic stress equations for the particulate phase from the given equation of motion for a single particle (i.e., from "first principles"). As a bonus, the dispersion coefficients and coupling terms to the carrier fluid follow automatically in the form of time integrals over the particle paths.[1] For the purpose of application, we need to introduce suitable approximations in order to resolve the time integrals into simple algebraic expressions in terms of fluid–turbulence stresses and correlation times. A central point in the current paper is to evaluate and test these approximations.

The PIV and PTV data are used to calculate statistical estimates of the exact force correlation functions that control the dispersion tensors. These results are used to evaluate the approximate dispersion tensors that are adopted in the model, where the correlation functions are replaced by simple exponential forms with characteristic correlation times. The fluid–turbulence data are taken as input to the model, and the model output is compared to measured profiles of particle concentration and kinetic stress.

More *ad hoc* types of closure relations for the dispersion coefficients must be invoked in models based on Reynolds averaged equations for the particulate phase (e.g., Young and Leeming, 1997; Kataoka and Serizawa, 1989; Elghobashi and Abou-Arab, 1983), or "k–ϵ" approaches (e.g., Wang et al., 1997 and the modelling reviewed by Lightstone and Hodgson, 2004). Other Eulerian formulations that are based on kinetic theory similar to that of Reeks and Swailes, are due to Simonin (2000), Zaichik and Alipchenkov (2005). Caraman et al. (2003) applied Simonin's modelling approach to analyze gas–solids flow, including particle collisions.

[1] The general integrals provide exact closures for the dispersion coefficients if the turbulent force acting on the particles is Gaussian. The dispersion tensors are therefore approximate in non-Gaussian cases, such as in near-wall regions.

In the original version of the kinetic theory (Reeks, 1992), a dilute suspension is considered where the particles do not interact. In the current work, we extend the Eulerian equations to account for particle–particle hydrodynamic interactions. This is implemented by adopting a collisional term in the stress equations, following Simonin (2000) and Caraman et al. (2003). Close range electrostatic particle–particle interactions that may occur in particle beds and dense suspensions are not accounted for in the current model.

1.2. Overview of the experiments

A series of experiments were conducted in the Hydrodynamics Laboratory at the University of Oslo to provide support for the modelling work. A detailed description of the experimental work is found in Drazen and Jensen (in preparation), while an additional description of the experimental work with a focus on turbulence enhancement can be found in Drazen and Jensen (2007). The aim of the experiments was to simultaneously measure the properties of both phases in a solid–liquid pipe flow. The facility consists of a 50 mm ID perspex pipe with a length of 30 m (Fig. 1). At one end of the pipe there are separation tanks with a set of ball valves through which the particulate phase was introduced into the flow via a Venturi. The solid phase consisted of 950 μm polystyrene beads ($\rho_p = 1.05\ \mathrm{g\ cm^{-3}}$) while the liquid phase was water. The mean volume fraction of particles was $\Phi \approx 0.003$.

Data were collected over pipe Reynolds numbers ranging from 40,000 to 115,000. The images were recorded using a high-speed camera capable of recording up to 2000 fps at 1024×1024 pixels, with a faster rate using reduced resolution. The particulate and carrier phases were separated using a median filtering technique based on the work of Kiger and Pan (2000). After separation, processing of the velocity data and particle positions was performed using Digiflow, a commercially available software package from Dalziel Research Partners.

Both the local fluid velocity and fluid acceleration along the particle tracks are needed to test the adopted dispersion coefficients in the Eulerian equations. To compute the fluid acceleration the technique of Jensen and Pedersen (2004) was used, yielding the total derivative of the fluid velocity, $D\mathbf{u}/Dt = \partial\mathbf{u}/\partial t + \mathbf{u}\cdot\nabla\mathbf{u}$. Individual particle tracks were generated from the particle position data returned by Digiflow, and the fluid velocity and acceleration values were interpolated onto the particle tracks.

The paper starts in Section 2 with a derivation of the Eulerian equations, with account for particle–particle interactions and tur-

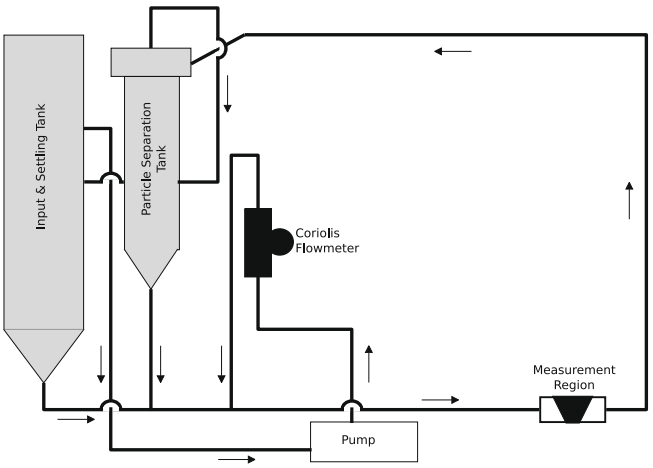

Fig. 1. Simplified schematic of the pipe flow facility at the Hydrodynamics Laboratory at the University of Oslo. The arrows denote the direction of flow.

bulent drag and added mass forces. In Section 4 we discuss the fluid–turbulence parameters that are extracted from the PIV/PTV data in order to provide the necessary model input. The model results with regard to particle stress and concentration profiles, are summarized in Section 5. The discussion and conclusion follow in Section 6.

2. The particle equation of motion

2.1. Drag and added mass forces

Maxey and Riley (1983) derived the equation of motion (EOM) for a particle in a fluid in the limit of low particle Reynolds number ($Re_p \ll 1$). We will neglect history effects and the Faxen curvature effect, and adopt the following EOM:

$$m_p\dot{\mathbf{v}} = \frac{m_p}{\hat{\tau}_p}(\mathbf{u}-\mathbf{v}) + (m_p - m_f)\mathbf{g} + m_f\frac{D\mathbf{u}}{Dt} - \frac{1}{2}m_f\left[\dot{\mathbf{v}} - \frac{D\mathbf{u}}{Dt}\right] + \mathbf{f}_c, \tag{1}$$

where $\mathbf{v}$ is the particle velocity. We assume that this equation holds also for higher Reynolds numbers (larger than unity), although an additional Saffman-type lift force depending on local fluid vorticity might be relevant. The particle diameter is $d = 950\ \mu\text{m}$, $V_p = 4/3\pi(d/2)^3$ is the particle volume, $m_p = \rho_p V_p$ is the particle mass, where $\rho_p = 1.05\ \text{g/cm}^3$, $m_f = \rho_f V_p$ is the fluid mass displaced by the particle (where for water $\rho_f = 1.0\ \text{g/cm}^3$). The fluid velocity evaluated at the particle position is $\mathbf{u}$, and $\mathbf{g}$ is gravity. The particle relaxation time $\hat{\tau}_p(\mathbf{u},\mathbf{v})$ depends on the local drag coefficient and the local particle and fluid velocities. $D\mathbf{u}/Dt$ is the fluid acceleration evaluated at the particle position.

The "added mass term" is

$$-\frac{1}{2}m_f\left[\dot{\mathbf{v}} - \frac{D\mathbf{u}}{Dt}\right] \tag{2}$$

and

$$m_f\frac{D\mathbf{u}}{Dt}$$

accounts for viscous stress and pressure gradients in the fluid, acting on the particle surface. Auton et al. (1988) have shown that the added mass force on a sphere should be expressed in the form given in (2). The force due to hydrodynamic interaction is included formally via the force $\mathbf{f}_c$ that accounts for the perturbations due to the fluid velocity field induced by nearby particles. We will discuss this force in more detail below.

For adaption to the kinetic theory, we recast the EOM on the more convenient form

$$\dot{\mathbf{v}} = \frac{1}{\tau_p}(\mathbf{u}-\mathbf{v}) + \mathbf{g}_e + \alpha\frac{D\mathbf{u}}{Dt} + \mathbf{C} \tag{3}$$

with the following definitions:

$$\tau_p = \hat{\tau}_p(\mathbf{u},\mathbf{v})\left(1 + \frac{1}{2}\frac{\rho_f}{\rho_p}\right),$$

$$\mathbf{g}_e = \mathbf{g}\left(\frac{1-\frac{\rho_f}{\rho_p}}{1+\frac{1}{2}\frac{\rho_f}{\rho_p}}\right),$$

$$\alpha = \frac{\frac{3}{2}\frac{\rho_f}{\rho_p}}{1+\frac{1}{2}\frac{\rho_f}{\rho_p}},$$

$$\mathbf{C} = \frac{\mathbf{f}_c}{m_p\left(1+\frac{1}{2}\frac{\rho_f}{\rho_p}\right)}.$$

These relations account for the "trivial" added mass effects. The "non-trivial" part is due to the effect of the fluid acceleration on the particle diffusivity, as shown in Section 3.4.

The relaxation time $\hat{\tau}_p(\mathbf{u},\mathbf{v})$ is a local, stochastic quantity in turbulent flow. The current form of the kinetic theory requires that the particle force is proportional to the fluid velocity (for drag) or to the fluid acceleration (for the added mass effect). Thus, a constant relaxation time is required. We will therefore replace $\hat{\tau}_p$ with a relaxation time accounting for a characteristic particle Reynolds number Re_p,

$$(\tau_p)_{Re_p} = \frac{4}{3}\frac{\rho_p}{\rho_f}\frac{d_p^2}{\nu Re_p C_D}, \tag{4}$$

$$Re_p = \frac{d\overline{|\mathbf{u}-\mathbf{v}|}}{\nu}, \tag{5}$$

$$C_D = \frac{24}{Re_p}\left(1 + 0.15Re_p^{0.687}\right) \quad \text{for } Re_p \leqslant 1000, \tag{6}$$

$$C_D = 0.44 \quad \text{for } Re_p > 1000, \tag{7}$$

where ν is the kinematic viscosity of the fluid (for water $\nu = 10^{-6}\ \text{m}^2/\text{s}$), and $\overline{|\mathbf{u}-\mathbf{v}|}$ is a characteristic average slip velocity along the particle paths. The correlation for the drag coefficient C_D, is in a standard form (e.g., Sommerfeld, 2003). We will not account for any modification due to turbulence of the ambient fluid. The relaxation time reduces to the Stokesian value

$$(\tau_p)_s = (\rho_p/\rho_f)d^2/(18\nu)$$

for $Re_p \to 0$, which is generally larger than $(\tau_p)_{Re_p}$. The final relaxation time we adopt, that is corrected for added mass, becomes

$$\tau_p = (\tau_p)_{Re_p}\left(1 + \frac{1}{2}\frac{\rho_f}{\rho_p}\right). \tag{8}$$

In the kinetic description we will frequently use the inverse time $\beta = \tau_p^{-1}$, which serves as a frictional drag coefficient.

2.2. Measured added mass effects

For the purpose of measuring the degree of correlation between the measured particle acceleration and the forcing terms, we rearrange the EOM,

$$\underbrace{\left(m_p + \frac{1}{2}m_f\right)\dot{\mathbf{v}}}_{\mathbf{a}_p} = \underbrace{\frac{m_p}{\hat{\tau}_p}(\mathbf{u}-\mathbf{v})}_{\mathbf{d}} + \underbrace{\frac{3}{2}m_f\frac{D\mathbf{u}}{Dt}}_{\mathbf{a}_f} + \underbrace{(m_p - m_f)\mathbf{g}}_{\mathbf{a}_g} + \mathbf{f}_c. \tag{9}$$

We can then calculate correlations between the acceleration and individual terms on the RHS of the equation. Assuming that the collision and gravitation terms are small, we expect a significant response in the cross-correlations $\langle(a_f)_i(a_p)_i\rangle$ and $\langle d_i(a_p)_i\rangle$ between equal Cartesian components i.

The first cross-correlation would demonstrate the contribution from the fluid acceleration or added mass forcing, and the second will measure the contribution from the drag-force. We will expect that the hydrodynamic interaction force $\mathbf{f}_c$ between particles is more important towards the pipe floor where the concentration is larger, introducing more noise there in $\mathbf{a}_p$. The gravitation introduces a constant offset in $\mathbf{a}_p$. Figs. 2 and 3 show cross-correlations and corresponding scatterplots for $\langle d_x(dv_x/dt)\rangle \sim \langle d_x(a_p)_x\rangle$ and $\langle Du_x/Dt(dv_x/dt)\rangle \sim \langle(a_f)_x(a_p)_x\rangle$ obtained form the experimental data, for the two larger Reynolds numbers. We will use x for the axial direction along the pipe, and y for the radial direction normal to the pipe walls.

We see a non-zero cross-correlation for both terms, with maximum correlation at positive time lag $\Delta t > 0$, in the sense $\langle A(t)B(t+\Delta t)\rangle$. The noise seen in each scatterplot is due to the data reduction procedure for the PIV and PTV data, the interaction force $\mathbf{f}_c$, and the terms in the EOM that are not included in the specific correlation at hand. The sloping lines in the scatterplots show an estimate of the principal axis. The ratio between the correlation maxima and principal axes, suggest that the fluid acceleration term

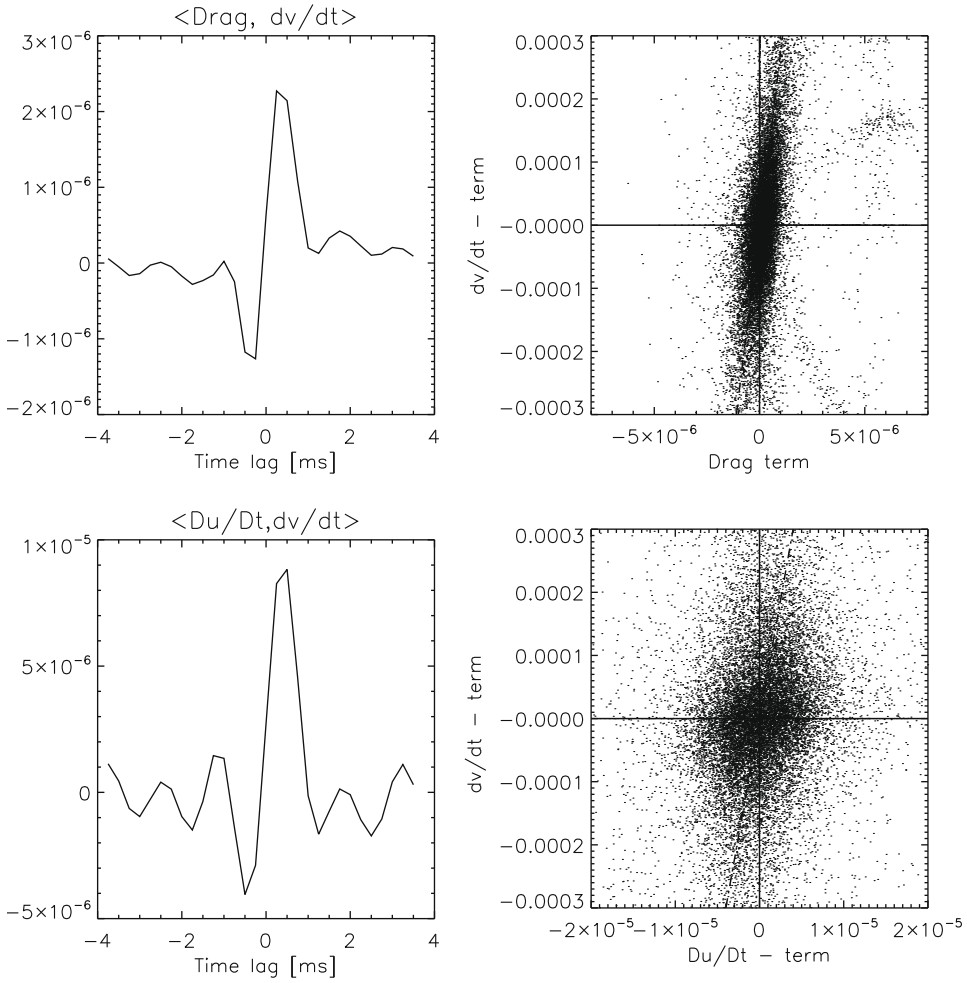

Fig. 2. Correlation between particle acceleration and force terms in the x-direction for $Re = 63,900$. The left panels show the cross correlation, and the right panels the scatterplot at the time lag of maximum correlation. The upper panels show $\langle d_x(dv_x/dt)\rangle$ and the bottom panels $\langle Du_x/Dt(dv_x/dt)\rangle$. The sloping lines in the scatterplots show estimates of the principal axis. The correlation with the acceleration term is about four times larger than the correlation with the drag term, showing that the added mass effect is significant.

provides a significantly larger contribution to the particle acceleration than the drag term. For the *y*-direction (not shown), the acceleration measurements are subject to more noise, and we cannot see a clear correlation between particle and fluid accelerations in the current dataset.

3. The kinetic model

3.1. Kinetic theory for a collisionless, dilute suspension

3.1.1. The PDF-equation and the dispersion tensors

The evolution (in phase space) of the ensemble averaged particle probability distribution function $\mathcal{P} = \langle W(\mathbf{v},\mathbf{x},t)\rangle$ is governed by (e.g., Reeks, 1992, 1993; Hyland et al., 1999)

$$\partial_t \mathcal{P} + \mathbf{v}\cdot\nabla_{\mathbf{x}}\mathcal{P} + \nabla_{\mathbf{v}}\cdot[(\mathbf{F}-\beta\mathbf{v})\mathcal{P}] = -\nabla_{\mathbf{v}}\cdot\mathscr{J}, \tag{10}$$

where the diffusion current is

$$\mathscr{J} = \langle \mathbf{f}W\rangle. \tag{11}$$

This equation is analogous to the classical Boltzmann equation (but now with the collision term replaced by the divergence of the diffusion current). The force components **f** and **F** represent the fluctuating and non-fluctuating fluid forces on the particle respectively (without collisions). Thus, the force terms in the EOM (3) imply that

$$\mathbf{f} = \frac{1}{\tau_p}(\mathbf{u}-\langle\mathbf{u}\rangle) + \alpha\frac{D\mathbf{u}}{Dt} - \alpha\left\langle\frac{D\mathbf{u}}{Dt}\right\rangle, \tag{12}$$

$$\mathbf{F} = \mathbf{g}_e + \frac{1}{\tau_p}\langle\mathbf{u}\rangle + \alpha\left\langle\frac{D\mathbf{u}}{Dt}\right\rangle, \tag{13}$$

where brackets denote ensemble averaging. *W* is the distribution function corresponding to a single realization of **f**.

For a Gaussian **f**, there is an exact closure relation for the diffusion current (Reeks, 1992, 1993),

$$\mathcal{J}_k = -\partial_{vj}(\mu_{jk}\mathcal{P}) - \partial_{xj}(\lambda_{jk}\mathcal{P}) - \gamma_k\mathcal{P} \tag{14}$$

in terms of three given dispersion tensors, μ_{jk}, λ_{jk} and γ_k which are functions of $(\mathbf{v},\mathbf{x},t)$. In the following Eulerian equations we will need the density weighted averages of the dispersion tensors, e.g.,

$$\overline{\lambda}_{ji}(\mathbf{x},t) = \int_{\mathbf{v}} \phi(\mathbf{v},\mathbf{x},t)\lambda_{ji}(\mathbf{v},\mathbf{x},t)d^3\mathbf{v},$$

$$\phi(\mathbf{v},\mathbf{x},t) = \frac{\mathcal{P}(\mathbf{v},\mathbf{x},t)}{\rho},$$

$$\rho(\mathbf{x},t) = \int_{\mathbf{v}} \mathcal{P}(\mathbf{v},\mathbf{x},t)d^3\mathbf{v}.$$

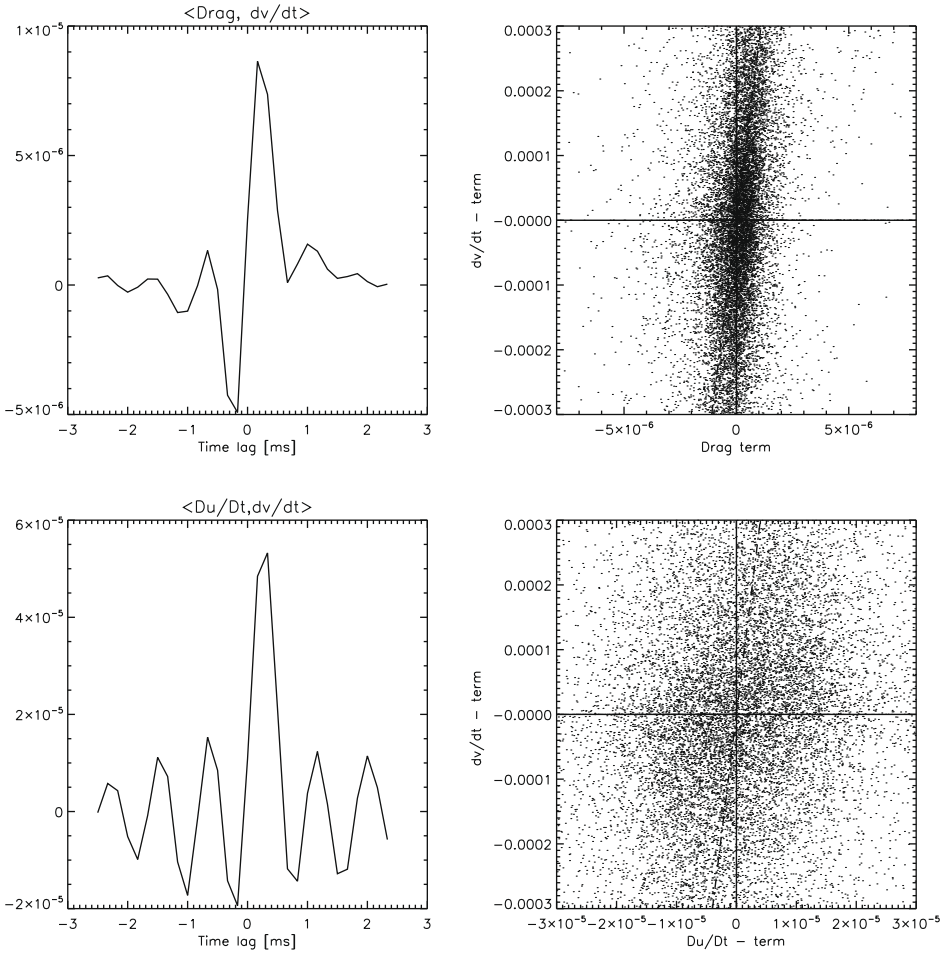

Fig. 3. Correlation between particle acceleration and force terms in the x-direction for $Re = 115,000$.

The dispersion tensor $\bar{\lambda}_{ji}$ may also be given in terms of the correlation between the local force $f_i(\mathbf{x}, t)$ and the total displacement $\Delta\mathbf{x}_j$ the particle experiences along its path, before it passes through $\mathbf{x}$ at time t (Reeks, 1992),

$$\bar{\lambda}_{ji} = \langle f_i(\mathbf{x}, t)\Delta x_j(\mathbf{x}, t)\rangle.$$

This can be understood in terms of small contributions to the displacement induced by the force on the particle along its path (sum of small contributions). It is only the recent history, within the correlation time of the driving force, that will contribute significantly to the correlation bracket. A similar correlation defines $\bar{\mu}_{ji}$, but in terms of the total velocity change along the particle path,

$$\bar{\mu}_{ji} = \langle f_i(\mathbf{x}, t)\Delta v_j(\mathbf{x}, t)\rangle.$$

The dispersion vector is given by

$$\bar{\gamma}_i = -\langle(\partial_j f_i(\mathbf{x}, t))\Delta x_j(\mathbf{x}, t)\rangle,$$

where summation over j is implied.

The velocity change and displacement is expressed in terms of Green's function of the EOM (or the response function). See Appendix C for the derivation of Green's function with added mass effects included. We will assume a linear mean shear in the background fluid, and the response function is then deterministic. The dispersion tensors then assume explicit forms directly in terms of the force correlation functions (e.g., Hyland et al., 1999),[2]

$$\bar{\lambda}_{ji} = \int_{-\infty}^{t} \langle f_i(\mathbf{x}, t) f_k(\mathbf{x}_p(s), s)\rangle G_{kj}(t - s)ds, \tag{15}$$

$$\bar{\mu}_{ji} = \int_{-\infty}^{t} \langle f_i(\mathbf{x}, t) f_k(\mathbf{x}_p(s), s)\rangle \dot{G}_{kj}(t - s)ds, \tag{16}$$

$$\bar{\gamma}_i = -\int_{-\infty}^{t} \langle(\partial_j f_i(\mathbf{x}, t)) f_k(\mathbf{x}_p(s), s)\rangle G_{kj}(t - s)ds. \tag{17}$$

The only known way to evaluate the dispersion tensors in wall bounded turbulence, is with the aid of Monte-Carlo simulations with particle tracking (e.g., Skartlien, 2007,b), or via direct numerical simulation with particle tracking. If one assumes homogeneous turbulence with a linear mean shear, these tensors can be calculated analytically giving a direct relation to the fluid Reynolds stresses. We will adopt this approach in the following as a "local approximation".

3.1.2. Moments and constitutive relations

By taking the first three velocity moments of the PDF-equation, one obtains the mass, momentum and stress conservation equations for the particles:

$$\partial_t \rho + \partial_k(\rho \bar{v}_k) = 0, \tag{18}$$

$$\rho D_t \bar{v}_i + \partial_k(\rho \overline{v'_k v'_i}) - \rho(F_i - \beta \bar{v}_i) = -\partial_k(\bar{\lambda}_{ki}\rho) - \bar{\gamma}_i \rho, \tag{19}$$

where F_i is an external force and $D_t = \partial_t + \overline{v_k}\partial_k$. Appendix A discusses the diffusion equation for ρ, that can be generated from the momentum equation. The stress equation is (Reeks, 1992; Swailes et al., 1998; Hyland et al., 1999; Sergeev et al., 2002)

[2] These asymptotic "long time" values are evaluated by ignoring the initial conditions.

$$\partial_t(\rho\overline{v_i'v_j'}) + \partial_k(\rho\bar{v}_k\overline{v_i'v_j'}) + \partial_k(\rho\overline{v_i'v_j'v_k'}) + 2\beta\rho\overline{v_i'v_j'} = \rho(\bar{\mu}_{ji} + \bar{\mu}_{ij}) - \rho(\mathcal{T}_{ik}\partial_k\bar{v}_j + \mathcal{T}_{jk}\partial_k\bar{v}_i) + \mathcal{R}_{ij}, \quad (20)$$

where

$$\mathcal{T}_{ik} = \overline{v_i'v_k'} + \bar{\bar{\lambda}}_{ki}, \quad (21)$$

$$\mathcal{R}_{ij} = -\partial_k[\rho(\overline{\lambda_{kj}v_i'} + \overline{\lambda_{ki}v_j'})] - \rho(\overline{\gamma_i v_j'} + \overline{\gamma_j v_i'}). \quad (22)$$

The terms $\mathcal{R}_{ij}$ are exactly zero with the models of the dispersion tensors used in this work (since we will assume they are independent of the velocity).

The constitutive relations emerge naturally from the theory. The particle stress tensor is given by

$$T_{ik} = \rho(\overline{v_i'v_k'} + \bar{\bar{\lambda}}_{ki}), \quad (23)$$

and the particle diffusivity tensor is

$$\epsilon_{ik} = \tau_p(\overline{v_i'v_k'} + \bar{\bar{\lambda}}_{ki}). \quad (24)$$

The diffusivity depends on particle inertia via τ_p, the particle kinetic stress, and also directly on the action of the background fluid via the dispersion tensor $\bar{\bar{\lambda}}_{ki}$. The dispersion tensor $\bar{\bar{\lambda}}_{ki}$ has two contributions in a wall bounded flow, namely the dispersion induced by the mean shear in the carrier flow, and the dispersion induced by the carrier turbulence (Reeks, 1993).

For the turbulent fluxes that enter in the stress equations, we apply the Chapman–Enskog closure relation (Swailes et al., 1998; Zaichik and Alipchenkov, 2005),

$$\overline{v_i'v_j'v_k'} = -\frac{1}{3}\left\{\epsilon_{in}\partial_n\overline{v_k'v_j'} + \epsilon_{jn}\partial_n\overline{v_k'v_i'} + \epsilon_{kn}\partial_n\overline{v_j'v_i'}\right\}, \quad (25)$$

in terms of the local particle diffusivities ϵ_{ik} given in (24). Note that this approximation serves as the required closure relation for the hierarchy of moments of the PDF-equation.

3.2. Kinetic stress equation with account for particle–particle interaction

With collisions, the kinetic PDF-equation (Section 3.1.1) generalizes to

$$\partial_t\mathcal{P} + \mathbf{v}\cdot\nabla_{\mathbf{x}}\mathcal{P} + \nabla_{\mathbf{v}}\cdot[(\mathbf{F} - \beta\mathbf{v})\mathcal{P}] = -\nabla_{\mathbf{v}}\cdot\mathscr{J} + (\partial_t\mathcal{P})_{\text{coll.}}, \quad (26)$$

where the diffusion current $\mathscr{J} = \langle\mathbf{f}W\rangle$ has the same meaning as before, with $\mathbf{f}$ the force due to turbulence. In the limit of zero fluid force (infinite relaxation time, $\beta \to 0$ and $\mathcal{J} \to 0$), we recover the classical Boltzmann equation.

In order to include collisional effects in the continuum equations for gas–particle flow, Simonin (2000) applied Grad's (1949) theory for rarefied gases where only two-particle interactions are accounted for. Simonin assumed uncorrelated particle velocities and elastic collisions as in Boltzmann's classical work. With these simplifying assumptions, the work of Jenkins and Richmann (1985) implies that the collisions only enter in the stress equations. Thus, the momentum equation (19) is unaltered, while the stress equation (20) should be replaced by

$$\partial_t(\rho\overline{v_i'v_j'}) + \partial_k(\rho\bar{v}_k\overline{v_i'v_j'}) + \partial_k(\rho\overline{v_i'v_j'v_k'}) + 2\beta\rho\overline{v_i'v_j'} = \rho(\bar{\mu}_{ji} + \bar{\mu}_{ij}) - \rho(\mathcal{T}_{ik}\partial_k\bar{v}_j + \mathcal{T}_{jk}\partial_k\bar{v}_i) + \mathcal{C}_{ij}, \quad (27)$$

where the collisional redistribution term is (Simonin, 2000; Caraman et al., 2003)

$$\mathcal{C}_{ij} = -\rho\frac{\sigma_c}{\tau_c}\left(\overline{v_i'v_j'} - \frac{2}{3}q_p^2\delta_{ij}\right), \qquad q_p^2 = \frac{1}{2}\left(\overline{v_x'v_x'} + \overline{v_y'v_y'} + \overline{v_z'v_z'}\right). \quad (28)$$

Here $\sigma_c = 4/5$ and the mean time between collisions is $\tau_c = 1/\nu_c$, where the collision frequency is

$$\nu_c = \pi n d^2\sqrt{\frac{16}{\pi}\frac{2}{3}q_p^2},$$

where $n = n(x,y,z)$ is the local particle number density. This model accounts for the effect that collisions dissipate the particle shear stress components and drive the normal stresses to equipartition. That is, the particle stresses become more isotropic, with reduced shear stress.

In particle–liquid flow, collisions are replaced by hydrodynamic interactions involving fluid dynamic effects upon close encounter between two or more particles. We will model the interactions by adopting Simonin's expressions for elastic collisions, but replace the particle cross section or diameter d by a larger cross section given by a characteristic hydrodynamic length scale, $d_h > d$. The collision frequency with interaction is then defined as

$$(\nu_c)_{\text{hyd}} = \pi n d_h^2\sqrt{\frac{16}{\pi}\frac{2}{3}q_p^2}, \quad (29)$$

adopting $\tau_c = 1/(\nu_c)_{\text{hyd}}$ in the stress coupling term $\mathcal{C}_{ij}$.

For Stokes flow, one can show that the velocity perturbation around a translating sphere in a quiescent liquid scales as d/r (r is the distance from the particle surface), based on the Oseen tensor and its extension for small but non-zero Re_p (Batchelor, 1967). A reduction of the perturbed velocity in the surrounding fluid to a 20% level, corresponds to $r = 5d$. We find that $d_h \sim 6d$ yield results that are comparable to the experimental data, giving a substantial increase in the collision frequency $[(\nu_c)_{\text{hyd}} \sim 36\nu_c]$. We expect that Oseen's relation is a good approximation for translation in a turbulent fluid, when d is significantly smaller than the Kolmogorov length.

The importance of collisions/hydrodynamic interaction relative to that of turbulent forcing can be evaluated from the factor $\tau_p/\tau_c = \tau_p(\nu_c)_{\text{hyd}}$. For a strictly dilute flow, where collisions can be neglected, we would require $\tau_p/\tau_c \ll 1$. The volume fraction of particles may not represent the relevant parameter for judging the importance of interaction, due to long-range hydrodynamic interaction.[3]

Finally, it is important to note that the history of the turbulent force seen by a particle is influenced by collisions in the sense that the particle path is perturbed by the collisions. The altered particle path will potentially influence the value of the dispersion tensors (15)–(17). We will ignore this effect for the time being, but future research should address the collisional effect on the dispersion tensors.

3.3. Reduction to fully developed channel flow

The influence of gravity on the concentration profiles is quite strong (giving exponential profiles to first order), and as a first approximation one can assume constant particle concentration in horizontal planes. We therefore adopt channel flow equations to model the data (which is measured in a vertical plane or laser sheet through the center of the pipe). The model is then subject to upper and lower boundary conditions (see Fig. 4).

The PIV field of view covered about 1/2 pipe diameter for the two larger Reynolds numbers, and about 0.9 diameters for the smallest Reynolds number. Measured boundary values in the field of view served as boundary conditions for the model. Two Dirichlet kinetic stress conditions (upper and lower values) and one Dirichlet condition for the lower particle concentration, was taken from the data. We will later see that the kinetic stress equations reduce to local relations, such that the kinetic stress is insensitive to the boundary conditions.

[3] The "effective volume fraction" for interactions scales as $(d_h/d)^3 \gg 1$.

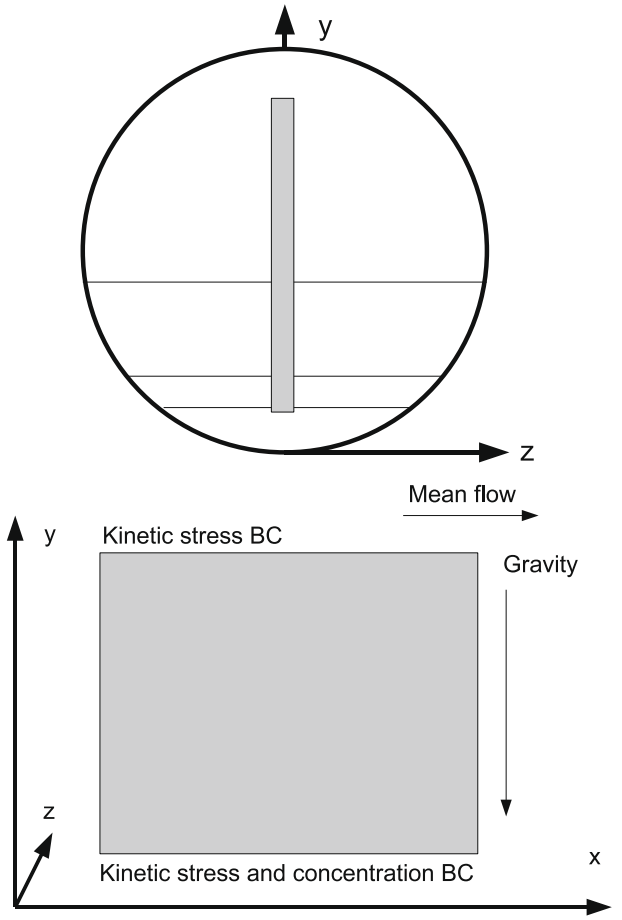

Fig. 4. (upper figure) Pipe cross section with schematic particle concentration contours. As first approximation one can assume constant particle concentration in horizontal planes, due to gravity. The PIV measurement plane is shown as a grey strip. (lower figure) Channel flow geometry adopted for the model. The two stress boundary conditions (upper and lower boundary), and one density boundary condition (lower boundary) are indicated. The PIV measurement area is indicated, with the accompanying model boundaries.

We will use the term "axial direction" for x (the direction of the mean flow), and "radial direction" for y (the wall normal direction), when we compare the data to model results. The spanwise direction in the model is z (corresponding to the azimuthal direction in the pipe). Gravity acts in the negative y-direction, perpendicular to the boundaries (see Fig. 4).

3.3.1. Components of the governing equations

In fully developed horizontal channel flow, $\partial_x(..) = \partial_z(..) = 0$ and $\partial_t(..) = 0$ for ensemble averaged quantities in general. Furthermore, $\bar{v}_y = \bar{v}_z = 0$. The mean force components on the particles per unit mass are

$$F_y = -g_e + \alpha\partial_y\langle u_y' u_y'\rangle, \tag{30}$$

$$F_x = \beta\langle u_x\rangle + \alpha\partial_y\langle u_x' u_y'\rangle \simeq \beta\langle u_x\rangle - \alpha\partial_y(\nu_t\partial_y\langle u_x\rangle), \tag{31}$$

$$F_z = 0, \tag{32}$$

for the wall normal, streamwise and spanwise components, respectively, and ν_t is the eddy viscosity. The term $\partial_y\langle u_y' u_y'\rangle$ is the gradient of the turbulence dynamic pressure per unit mass. The components of the momentum equation become

$$\begin{aligned}
&\partial_y(\rho\overline{v_y' v_y'}) + \rho(g_e - \alpha\partial_y\langle u_y' u_y'\rangle) = -\partial_y(\bar{\lambda}_{yy}\rho) - \bar{\gamma}_y\rho,\\
&\partial_y(\rho\overline{v_y' v_x'}) + \rho[\beta(\bar{v}_x - \langle u_x\rangle) - \alpha\partial_y\langle u_x' u_y'\rangle] = -\partial_y(\bar{\lambda}_{yx}\rho) - \bar{\gamma}_x\rho,\\
&\partial_y(\rho\overline{v_y' v_z'}) = -\partial_y(\bar{\lambda}_{yz}\rho) - \bar{\gamma}_z\rho.
\end{aligned} \tag{33}$$

Only the vertical component (33) is needed to solve for the concentration profile $\rho(y)$, with given $\bar{\lambda}_{yy}, \bar{\gamma}_y$, and a solution for the normal stress $\overline{v_y' v_y'}$. The formal solution for the concentration profile is

$$\rho(y) = \rho(0)\frac{\epsilon_{yy}(0)}{\epsilon_{yy}(y)}\exp\left\{-\tau_p\int_0^y \frac{g_e - \alpha\partial_y\langle u_y' u_y'\rangle + \bar{\gamma}_y}{\epsilon_{yy}}\,d\zeta\right\}, \tag{34}$$

where ϵ_{yy} is the normal component of the particle diffusivity (24). For the special case of homogeneous turbulence, ϵ_{yy} is constant and $\bar{\gamma}_y = 0$, such that an exponential profile is recovered.

The wall normal and axial components of the stress equation are, respectively,

$$\partial_y(\rho\overline{v_y' v_y' v_y'}) + 2\beta\rho\overline{v_y' v_y'} = 2\rho\bar{\mu}_{yy} - \rho\frac{\sigma_c}{\tau_c}\left(\overline{v_y' v_y'} - \frac{2}{3}q_p^2\right), \tag{35}$$

$$\partial_y(\rho\overline{v_x' v_x' v_y'}) + 2\beta\rho\overline{v_x' v_x'} = 2\rho\bar{\mu}_{xx} - 2\rho\mathcal{T}_{xy}\partial_y\bar{v}_x - \rho\frac{\sigma_c}{\tau_c}\left(\overline{v_x' v_x'} - \frac{2}{3}q_p^2\right). \tag{36}$$

The wall normal stress is needed for (33) (or the concentration profile 34), and for comparison with the stress data. The axial stress is calculated solely for comparison with the axial stress data. The stress equations are coupled via the collision term, but we will solve each of them independently, using measured data for the stress component we are not solving for. Likewise, we will use the measured shear stress in the calculation of $\mathcal{T}_{xy}$, rather than solving the shear stress equation.

For the axial stress $\overline{v_x' v_x'}$, the mean shear $\partial_y\bar{v}_x$ acts as an internal source. The collisional terms may act as sources or sinks. For air–particle flow in pipes or jets, it has been reported (e.g., Caraman et al., 2003) that collisions provide a sink for the axial stress and a source for the two other normal components. In the current case, the shear induced source for the axial stress is not important, but the stress redistribution effect due to hydrodynamic interaction needs to be included to match the measurements.

3.3.2. Local approximation of the stress equations

When the turbulent flux terms can be neglected, the set of stress equations above reduce to the local algebraic relations

$$2\beta\rho\overline{v_y' v_y'} = 2\rho\bar{\mu}_{yy} - \rho\frac{\sigma_c}{\tau_c}\left(\overline{v_y' v_y'} - \frac{2}{3}q_p^2\right), \tag{37}$$

$$2\beta\rho\overline{v_x' v_x'} = 2\rho\bar{\mu}_{xx} - 2\rho\mathcal{T}_{xy}\partial_y\bar{v}_x - \rho\frac{\sigma_c}{\tau_c}\left(\overline{v_x' v_x'} - \frac{2}{3}q_p^2\right). \tag{38}$$

In the current case, these local stress equations hold, as we will see below. This simplifies the problem considerably relative to gas–solids or gas–droplet flow, since we do not need to specify stress boundary conditions, and solve the differential equations. The turbulent flux is significant for large Stokes number gas–particle flow, and we must then revert to the coupled set of differential equations (35) and (36).

3.4. Local dispersion tensors with added mass effects

3.4.1. Correlation functions for the particle forces

A number of dispersion tensor components are required in the momentum and stress equations. These are in general given by the integrals (15)–(17), were the two-point temporal correlation function of the fluctuating part of the fluid force is required. With the definitions

$$f_i = d_i + a_i, \tag{39}$$

$$d_i = \beta u_i', \tag{40}$$

$$a_i = \alpha\left(\frac{D\mathbf{u}}{Dt}\right)_i', \tag{41}$$

the desired two-point correlation function can be expressed as

$$\begin{aligned}
\langle f_i(\mathbf{x},t)f_k(\mathbf{x}_p(s),s)\rangle =& \langle d_i(\mathbf{x},t)d_k(\mathbf{x}_p(s),s)\rangle + \langle a_i(\mathbf{x},t)a_k(\mathbf{x}_p(s),s)\rangle\\
&+ \left[\langle d_i(\mathbf{x},t)a_k(\mathbf{x}_p(s),s)\rangle + \langle a_i(\mathbf{x},t)d_k(\mathbf{x}_p(s),s)\rangle\right].
\end{aligned} \tag{42}$$

Brackets mean ensemble averaging over all $\mathbf{x}_p(s)$ *for fixed* $s < t$ belonging to paths converging to $\mathbf{x}$ at t (thus, brackets mean averaging over a set of different spatial positions $\mathbf{x}_p$). We will use the compact notation

$$R_{ik}^{mn}(y,t,s) = \langle m_i(\mathbf{x},t) n_k(\mathbf{x}_p(s),s)\rangle \tag{43}$$

for the individual contributions, replacing (42) with

$$\langle f_i f_k\rangle = \sum_m \sum_n R_{ik}^{mn} = R_{ik}^{dd} + R_{ik}^{ad} + R_{ik}^{da} + R_{ik}^{aa}. \tag{44}$$

Here, m and n refers to force type (d or a) and i,k refers to coordinate directions (x or y in our case).

We assume that the two-point correlations R_{ij}^{mn} can be expressed in terms of a time dependent exponential decay of the corresponding local single-point correlation. In the case of channel flow, the "locally homogeneous approximation" is

$$R_{ik}^{mn}(y,t,s) = Q_{ik}^{mn}(y) e^{-(t-s)/\tau_{ik}^{mn}(y)}, \tag{45}$$

where the local force correlations are

$$Q_{ik}^{mn}(y) = \langle m_i(y) n_k(y)\rangle. \tag{46}$$

We calculate $R_{ik}^{mn}(y,t,s)$ from the combined PTV/PIV data. These correlation functions are then fitted with exponentials to calculate the timescales $\tau_{ik}^{mn}(y)$. The different τ_{ik}^{mn} may not vary very much over different combinations of i and k, so we replace this tensor with a characteristic scalar value τ_{mn} when appropriate,

$$R_{ik}^{mn}(y,t,s) \simeq Q_{ik}^{mn}(y) e^{-(t-s)/\tau_{mn}(y)}. \tag{47}$$

We will use the full profiles $Q_{ik}^{mn}(y)$, but single characteristic values τ_{mn} for the timescales, as input to the model.

3.4.2. Dispersion tensor components

Only the components that we need for the subsequent calculations are given below. Appendix B provides the necessary details for the dispersion tensor calculations, and explains the approximations that are adopted. The $\bar{\mu}$ components are given by the scaling in (D.2), once the $\bar{\lambda}$-components are calculated. The $\bar{\lambda}$-components that are needed in the wall normal momentum and stress equations are

$$(\bar{\lambda}_{yy})_{dd} = Q_{yy}^{dd} \frac{\tau^2}{1+\beta\tau - \alpha C''_{yy}\tau^2}, \tag{48}$$

$$(\bar{\lambda}_{yy})_{ad} \simeq 0, \tag{49}$$

$$(\bar{\lambda}_{yy})_{aa} = Q_{yy}^{aa} \frac{\tau_{aa}^2}{1+\beta\tau_{aa} - \alpha C''_{yy}\tau_{aa}^2}, \tag{50}$$

The streamwise components that are needed in the axial stress equation are

$$(\bar{\lambda}_{xx})_{dd} = \frac{\tau^2}{1+\beta\tau}\left(Q_{xx}^{dd} + B_1 Q_{xy}^{dd}\frac{\tau^2}{1+\beta\tau - \alpha C'_{yy}\tau^2}\right), \tag{51}$$

$$(\bar{\lambda}_{xx})_{ad} = \frac{\tau_{ad}^2}{1+\beta\tau_{ad}}\left(Q_{xx}^{ad} + B_1 Q_{xy}^{ad}\frac{\tau_{ad}^2}{1+\beta\tau_{ad} - \alpha C''_{yy}\tau_{ad}^2}\right), \tag{52}$$

$$(\bar{\lambda}_{xx})_{aa} = \frac{\tau_{aa}^2}{1+\beta\tau_{aa}}\left(Q_{xx}^{aa} + B_1 Q_{xy}^{aa}\frac{\tau_{aa}^2}{1+\beta\tau_{aa} - \alpha C''_{yy}\tau_{aa}^2}\right). \tag{53}$$

And the "shear components" that are needed in the axial stress equation are

$$(\bar{\lambda}_{yx})_{dd} = Q_{xy}^{dd} \frac{\tau^2}{1+\beta\tau - \alpha C''_{yy}\tau^2}, \tag{54}$$

$$(\bar{\lambda}_{yx})_{ad} = Q_{xy}^{ad} \frac{\tau_{ad}^2}{1+\beta\tau_{ad} - \alpha C''_{yy}\tau_{ad}^2}, \tag{55}$$

$$(\bar{\lambda}_{yx})_{aa} = Q_{xy}^{aa} \frac{\tau_{ad}^2}{1+\beta\tau_{aa} - \alpha C''_{yy}\tau_{aa}^2}. \tag{56}$$

The correlation tensors in (48)–(56) are given by

$$Q_{yy}^{dd} = \beta^2\langle u'_y u'_y\rangle, \tag{57}$$

$$Q_{xx}^{dd} = \beta^2\langle u'_x u'_x\rangle, \tag{58}$$

$$Q_{xy}^{dd} = \beta^2\langle u'_x u'_y\rangle, \tag{59}$$

$$Q_{yy}^{aa} = \langle a_y a_y\rangle, \tag{60}$$

$$Q_{xx}^{aa} = \langle a_x a_x\rangle, \tag{61}$$

$$Q_{xy}^{aa} = \langle a_x a_y\rangle, \tag{62}$$

$$Q_{xx}^{ad} \simeq 2\alpha\beta\langle u'_x u'_y\rangle\partial_y\langle u_x\rangle, \tag{63}$$

$$Q_{xy}^{ad} \simeq \alpha\beta\langle u'_y u'_y\rangle\partial_y\langle u_x\rangle. \tag{64}$$

The approximations leading to the last two terms are explained in Appendix B. The auxiliary variables in (48)–(56) depend on added mass (via fluid stress gradients) and drag (via the mean shear),

$$B_1 = \beta\partial_y\langle u_x\rangle + \alpha C''_{xy},$$

$$C''_{xy} = \partial_y^2\langle u'_x u'_y\rangle,$$

$$C''_{yy} = \partial_y^2\langle u'_y u'_y\rangle.$$

4. Model parameters extracted from the data

The required model input is $Q_{ij}^{mn}(y)$ and the corresponding timescales τ_{dd}, τ_{ad} and τ_{aa}. These parameters are taken from the data. The relaxation time τ_p and the effective gravity g_e are determined by the fluid viscosity and density, the particle material density and particle Reynolds number. The latter is estimated from the dataset to calibrate the average drag coefficient.

4.1. Particle relaxation times

The average values of Re_p based on the time averaged velocity difference $\overline{|\mathbf{u}-\mathbf{v}|}$, for flow Reynolds numbers $Re = [43,000, 64,000, 115,000]$, were $Re_p = [65, 130, 180]$ respectively. This is below the vortex shedding threshold of $Re_p \simeq 300$ (Johnson and Patel, 1999) for translation in quiescent fluid, but well beyond the Stokes limit for the drag term. A relatively large standard deviation in the slip velocity (up to $\sim 70\%$) suggests that the particles shed vortices intermittently.

4.2. Measured drag and acceleration correlation times seen from particles

The dominating sources for the radial and axial normal kinetic stresses are associated with R_{yy}^{dd} and R_{xx}^{dd} respectively, and in particular the added mass terms R_{yy}^{ad} and R_{xx}^{ad}. Figs. 5–8 show these correlation functions, at a certain position in the pipe. The timescales for R_{yy}^{dd} and R_{xx}^{dd} are estimated directly from the data using exponential fits, and by averaging over all radial positions.[4]

The measured timescales for R_{yy}^{aa} and R_{xx}^{aa} are comparable to the sampling interval used (the sampling frequency was 2, 4 and 6 kHz, respectively, for the three Reynolds numbers, giving the sampling intervals $\Delta t = 0.5$, 0.25 and 0.16 ms). This resolution limitation is seen in Figs. 7 and 8. We will therefore treat the correlation times associated with the "aa" terms as tuning parameters, since they are not readily available from the data. We will also distinguish between the x- and y-direction for these correlation times, in order to obtain a reasonable fit to the magnitude of the measured particle kinetic stresses. Table 1 summarizes the timescales

[4] The PIV data window spans only about 1/2 of the pipe diameter for the two largest Reynolds numbers, so an average value seems a reasonable representation.

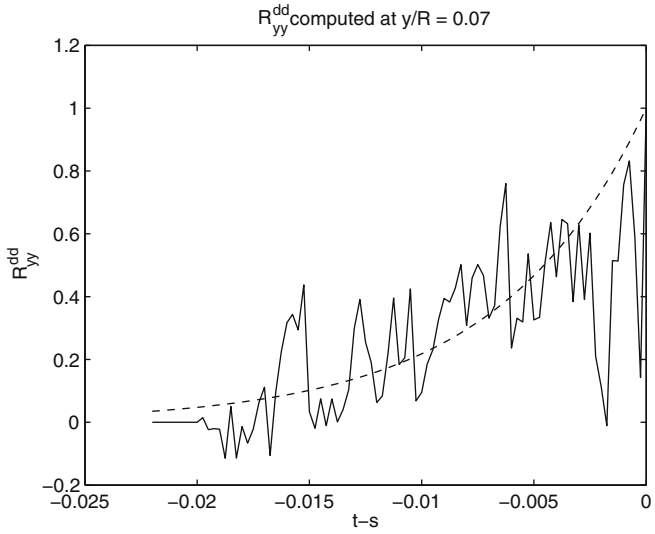

Fig. 5. Measured correlation function R^{dd}_{yy} for $Re = 63,900$. The time axis is in units of seconds. The correlation time is estimated from an exponential fit.

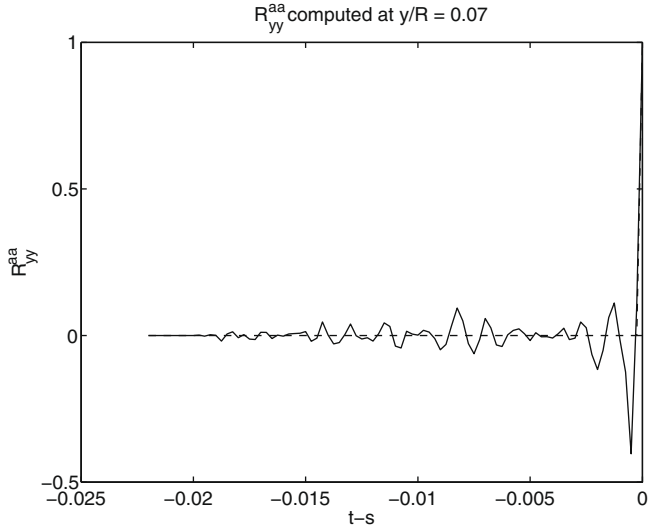

Fig. 7. Measured correlation function R^{aa}_{yy} for $Re = 63,900$. The correlation time is here unresolved with the sampling interval of $\Delta t = 0.25$ ms.

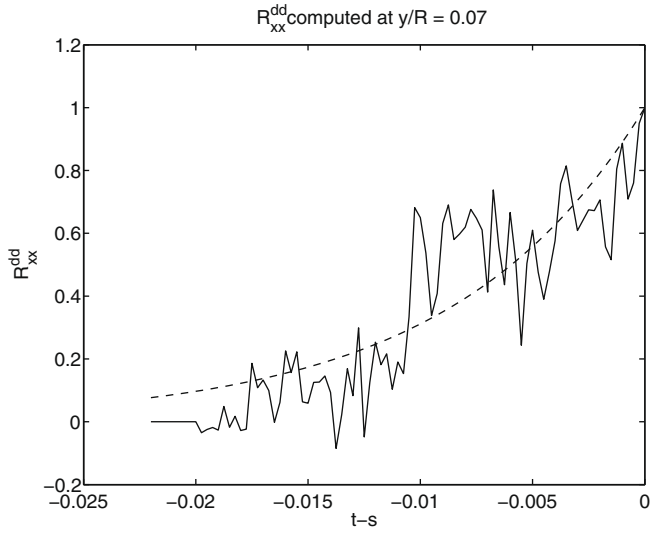

Fig. 6. Measured correlation function R^{dd}_{xx} for $Re = 63,900$. The time axis is in units of seconds. The correlation time is estimated from an exponential fit.

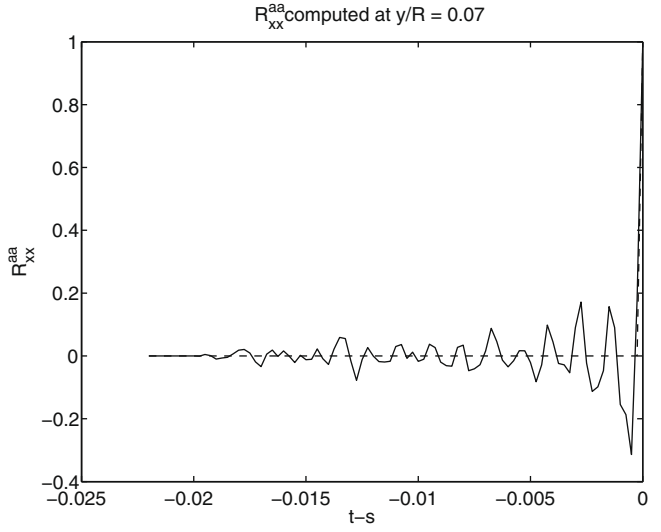

Fig. 8. Measured correlation function R^{aa}_{xx} for $Re = 63,900$. The correlation time is here unresolved with the sampling interval of $\Delta t = 0.25$ ms.

used as model input, in addition to estimates of Eulerian timescales of the turbulence.

The Stokes number is defined by the ratio of the particle inertial relaxation time to the drag correlation time. The Stokes numbers for all Reynolds numbers (Table 1) are larger than unity which indicates that the polystyrene particles cannot be treated as passive tracer particles, even though the density contrast between fluid and particles is very small.

4.3. Fluid timescales compared to τ_{dd}

The particle material density is a few percent larger than for water, such that the settling velocity is small compared to the characteristic turbulent velocity. Thus, the Csanady/crossing trajectories effect can be ignored. We expect that the fluid velocity correlation time τ_{dd} seen by the particles is still reduced compared to the Lagrangian correlation time of the fluid τ_L (not measured), due to the added mass force and particle–particle interactions. The Eulerian integral timescale τ_E for the radial velocity is also given in Table 1. This is a factor 3–5 smaller than τ_{dd}.

Table 1
The *upper rows* show the relaxation time τ_p corrected for the particle Reynolds number Re_p and added mass (Eq. (8)), the Stokes number based on $\tau = \tau_{dd}$, the Eulerian correlation time τ_f estimated from the eddy viscosity and the radial fluid stress, and τ_E the Eulerian correlation time of the radial fluid velocity component. The *lower rows* show the characteristic correlation times as seen by the particles. The correlation time for the fluid velocity is $\tau = \tau_{dd}$, the cross correlation time between the fluid acceleration and the fluid velocity is τ_{ad}. The two correlation times for the fluid acceleration, $(\tau_{aa})_{yy}$ and $(\tau_{aa})_{xx}$, are tuned parameters since the correlation functions were under-resolved.

Re	τ_p (ms)	Re_p	$St = \tau_p/\tau$	τ_f (ms)	τ_E (ms)
43,000	19.2	65	1.28	80	3.1
63,900	12.7	130	2.54	65	1.8
115,000	9.0	180	3.03	35	0.9
Re	τ (ms)	τ_{ad} (τ)	$(\tau_{aa})_{yy}$ (τ)	$(\tau_{aa})_{xx}$ (τ)	
43,000	15	0.10	0.10	0.10	
63,900	5	0.12	0.12	0.24	
115,000	3	0.06	0.06	0.24	

Another timescale that is frequently used is the eddy turnover time defined by the scalar diffusivity. Skartlien (2007, 2009) showed that the wall normal particle diffusivity for vanishing Stokes number, and for drag only, limits to

$$(\epsilon_{yy})_h = \langle u'_y u'_y \rangle \tau$$

when the locally homogeneous form of the dispersion tensor $\bar{\lambda}_{yy}$ is invoked. If we impose consistency between the eddy diffusivity and the wall normal particle diffusivity for vanishing relaxation time, we obtain the following eddy turnover time:

$$\tau_f = \nu_T / \langle u'_y u'_y \rangle, \tag{65}$$

where ν_T is the fluid eddy viscosity.

The eddy turnover time (given in Table 1) is about an order of magnitude larger than τ_{dd}. Thus, the needed correlation time τ_{dd} cannot be estimated by the eddy turnover time τ_f in the current setting, where the added mass effect is important. A better approximation is the Eulerian integral timescale τ_E, although this is a factor 3–5 smaller than τ_{dd}. The Lagrangian correlation time for the fluid, τ_L may be a better estimate.

4.4. Measured local force correlation tensors Q_{ij}^{mn}

We use the relations given in (57)–(64) on the dataset, to evaluate the local tensor components $Q_{ij}^{mn}(y)$. These correspond to the value of R_{ij}^{mn} at zero time lag. Vertical (or radial) profiles of a few measured correlation tensors for Re = 63,900 are given in Figs. 9 and 10, respectively. For the acceleration components Q_{xx}^{aa} and Q_{yy}^{aa} we adopt single characteristic values (average values over the pipe diameter) as the model input.

It is potentially convenient to have a relation between the acceleration components and the Reynolds stresses, since the acceleration components are not usually available in common modelling situations. We therefore define the following Eulerian acceleration timescales:

$$Q_{ii}^{aa} = \langle a_i a_i \rangle \equiv \alpha^2 \frac{\langle u'_i u'_i \rangle}{\hat{\tau}_i^2}, \tag{66}$$

$$Q_{xy}^{aa} = \langle a_x a_y \rangle \equiv \alpha^2 \frac{\langle u'_x u'_y \rangle}{\hat{\tau}_{xy}^2}. \tag{67}$$

These acceleration timescales are given in terms of the drag timescale τ_{dd} in Table 2, together with the characteristic values of Q_{ii}^{aa}. Further research may be necessary to incorporate more general relations between the Reynolds stresses and the acceleration statistics.

4.5. Collision frequency

We will now assess the importance of hydrodynamic interactions by invoking our simple collision model. The spanwise normal stress (in the line of sight of the camera used for PIV) is not available in the current data. We follow Caraman et al. (2003), and assume $\overline{v'_z v'_z} \simeq \overline{v'_y v'_y}$. The collision frequency is then modelled as

$$(\nu_c)_{\mathrm{hyd}} = \pi n d_h^2 \sqrt{\frac{16}{\pi}\frac{1}{3}\left(\overline{v'_x v'_x} + 2\overline{v'_y v'_y}\right)},$$

where n is the particle number density and d_h is the effective hydrodynamic interaction cross section.

The importance of particle–particle interactions relative to turbulent fluid forcing can be evaluated by comparing the collision time to the particle relaxation time. For a strictly dilute flow we would require $\tau_p(\nu_c)_{\mathrm{hyd}} \ll 1$, i.e., that the particle relaxes to the fluid motion before the next collision or interaction event. Fig. 11 shows in contrast that $\tau_p(\nu_c)_{\mathrm{hyd}}$ cannot be considered small, even

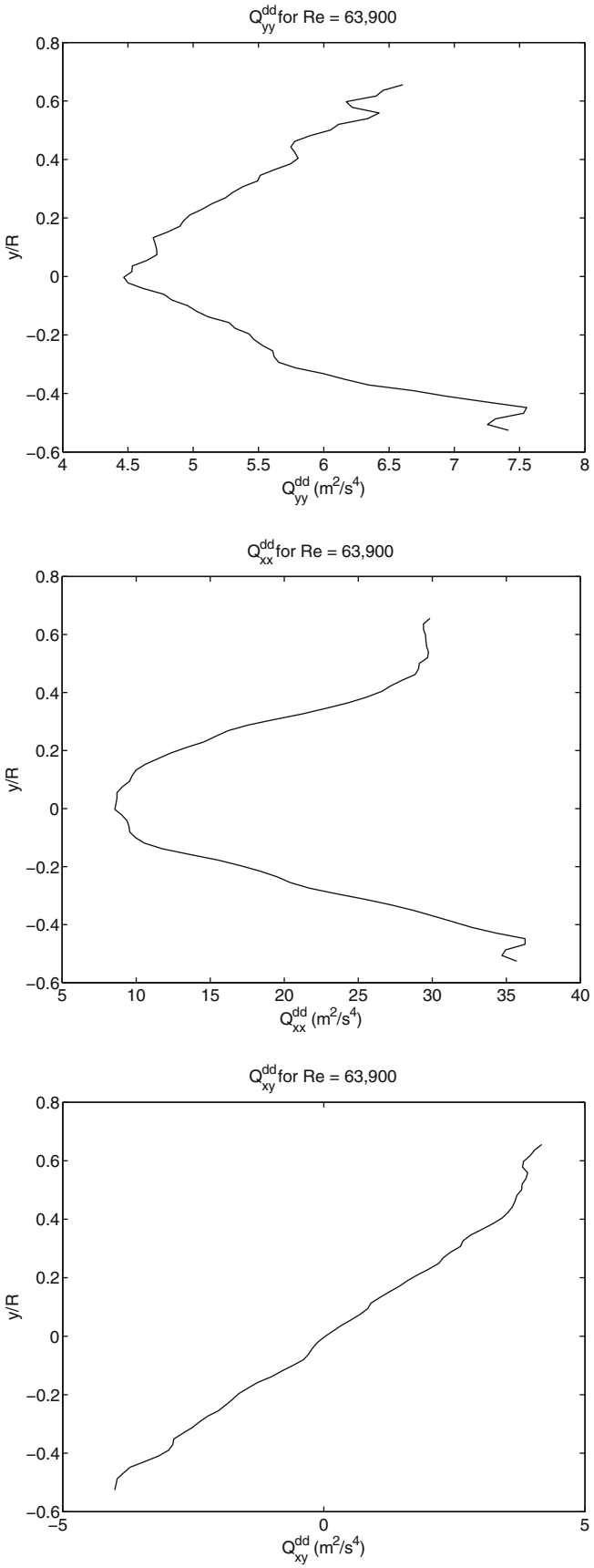

Fig. 9. Correlation functions $Q_{yy}^{dd}(y)$, $Q_{xx}^{dd}(y)$ and $Q_{xy}^{dd}(y)$ for $Re = 63,900$.

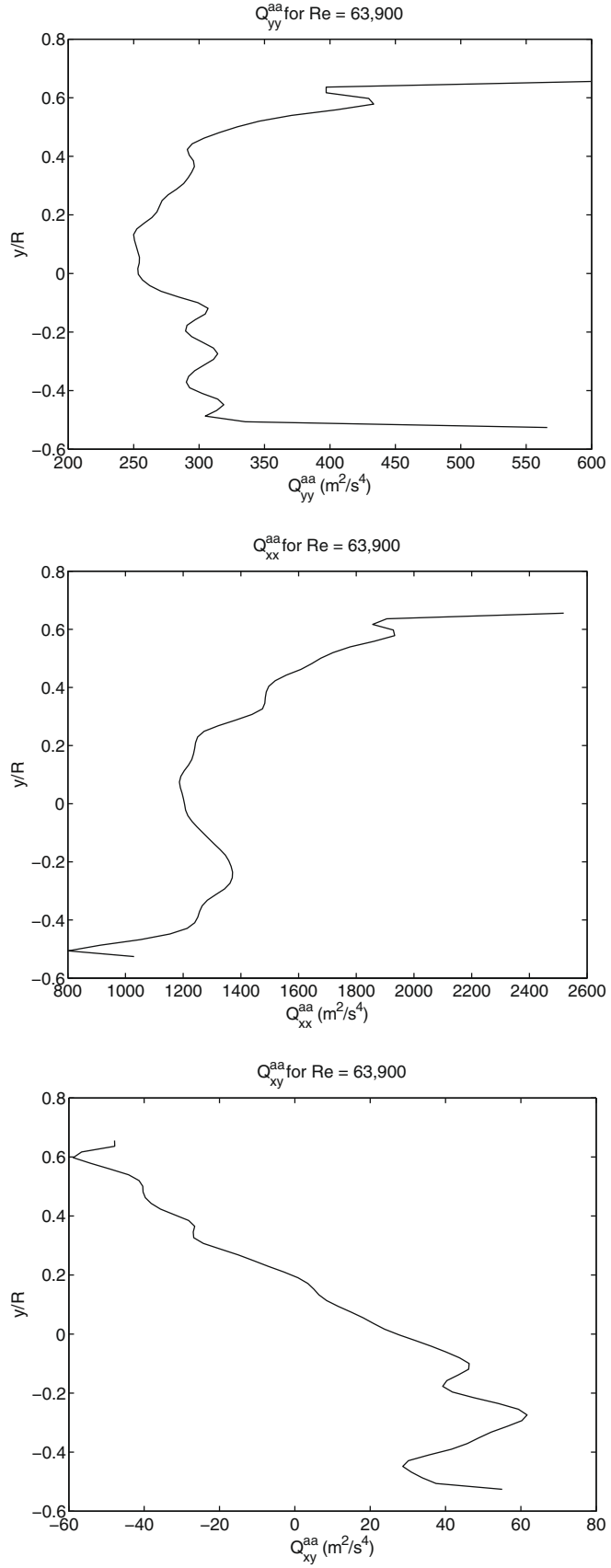

Fig. 10. Correlation functions $Q^{aa}_{yy}(y)$, $Q^{aa}_{xx}(y)$ and $Q^{aa}_{xy}(y)$ for $Re = 63,900$.

though the average volume fraction of particles is of the order 10^{-3}. We can therefore conclude that the flow is not strictly dilute.

Table 2
The Eulerian characteristic timescales of the fluid acceleration and measured characteristic values for Q^{aa}_{ii}.

Re	Q^{aa}_{yy} (m^2/s^4)	Q^{aa}_{xx} (m^2/s^4)	$\tilde{\tau}_y$	$\tilde{\tau}_x$	$\tilde{\tau}_{xy}$
43,000	50	250	0.2τ	0.2τ	0.3τ
63,900	300	1500	0.3τ	0.3τ	0.5τ
115,000	2500	9000	0.3τ	0.3τ	0.6τ

5. Model results

5.1. Concentration profiles using the measured particle kinetic stress

First, we solve (33) or (34) using a linear fit to the measured radial particle normal stress for $\langle v'_y v'_y \rangle$ and the local approximation for the dispersion tensors. With the PSA approximation for $\bar{\gamma}_y \simeq -\partial_y \bar{\lambda}_{yy}$ of Skartlien (2007) to ensure a well mixed condition in the limit of passive tracers, (33) reduces to

$$0 = -\epsilon_{yy}\partial_y \rho - \rho\tau_p \partial_y \overline{v'_y v'_y} - \rho\tau_p (g_e - \alpha \partial_y \langle u'_y u'_y \rangle), \tag{68}$$

where $-\epsilon_{yy}\partial_y\rho$ is the diffusive turbulent mass flux density, the wall normal diffusivity is $\epsilon_{yy} = \tau_p(\langle v'_y v'_y \rangle + \bar{\lambda}_{yy})$ and $-\rho\tau_p\partial_y\overline{v'_y v'_y}$ is the turbophoretic mass flux density. The diffusivity and turbophoretic flux is calculated using the measured kinetic stress $\langle v'_y v'_y \rangle$. The effective gravitational flux is $-\rho\tau_p(g_e - \alpha\partial_y\langle u'_y u'_y\rangle)$, corrected for turbulence pressure. Figs. 12–14 show the results for all Reynolds numbers.

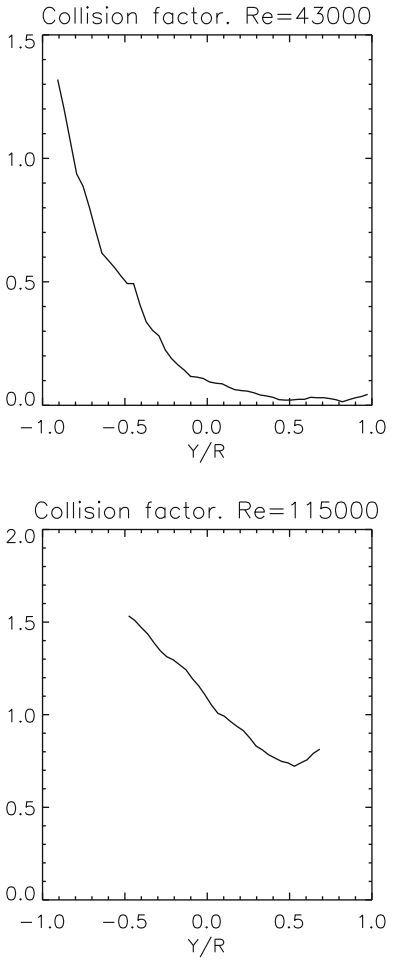

Fig. 11. Estimated collision factor $\tau_p v_c$ for $Re = 43,000$ and $Re = 115,000$, showing that the flow is not dilute, in particular towards the pipe floor.

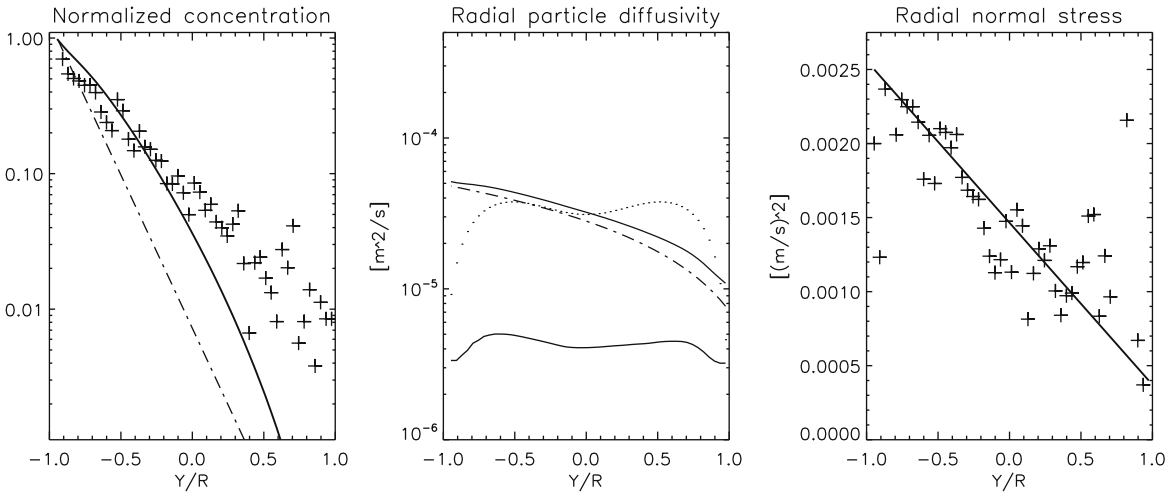

Fig. 12. Modelled concentration and radial diffusivity for *Re* = 43,000. The diffusivity is here based on the measured normal stress and the local dispersion tensor. (left panel) *Particle density profile:* (crosses) data; (thick line) model; (straight dash-dotted line) exponential profile using the mean diffusivity in the scale height $z_0 = \bar{\epsilon}_{yy}/V_T$. The profiles are normalized to the boundary value. (middle panel) *Particle diffusivity:* (full thick line) $\epsilon_{yy} = \tau_p\langle v'_y v'_y\rangle + \tau_p\bar{\lambda}_{yy}$; (dash-dotted thick line) $\tau_p\langle v'_y v'_y\rangle$; (dash-triple dotted line) $\tau_p\bar{\lambda}_{yy}$. The dotted line is the eddy viscosity (approximating the eddy diffusivity). (right panel) *Particle radial stress* $\langle v'_y v'_y\rangle$: The crosses represent the data and the thick full line is the linear fit.

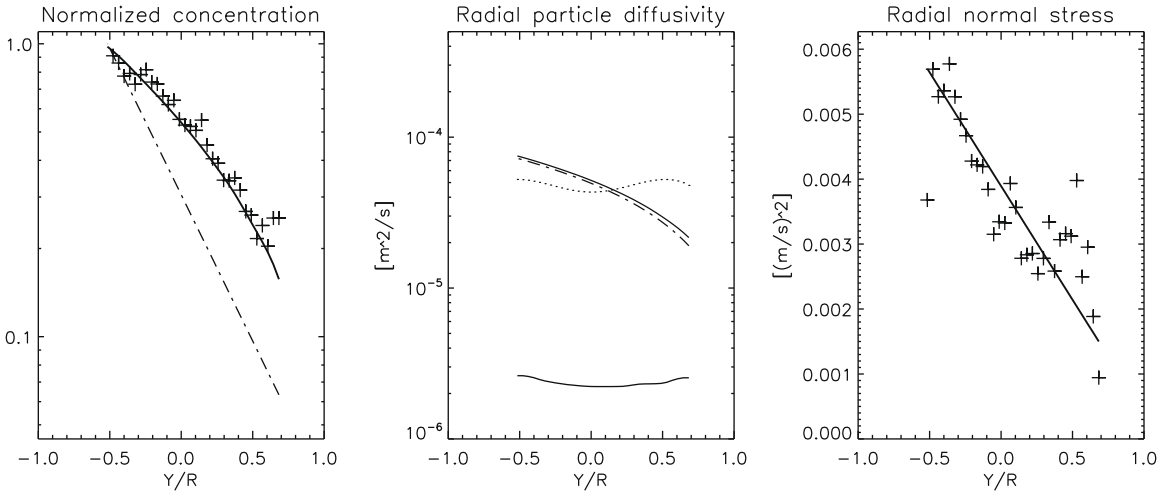

Fig. 13. Modelled concentration and radial diffusivity for Re = 63,900. The key is the same as in Fig. 12.

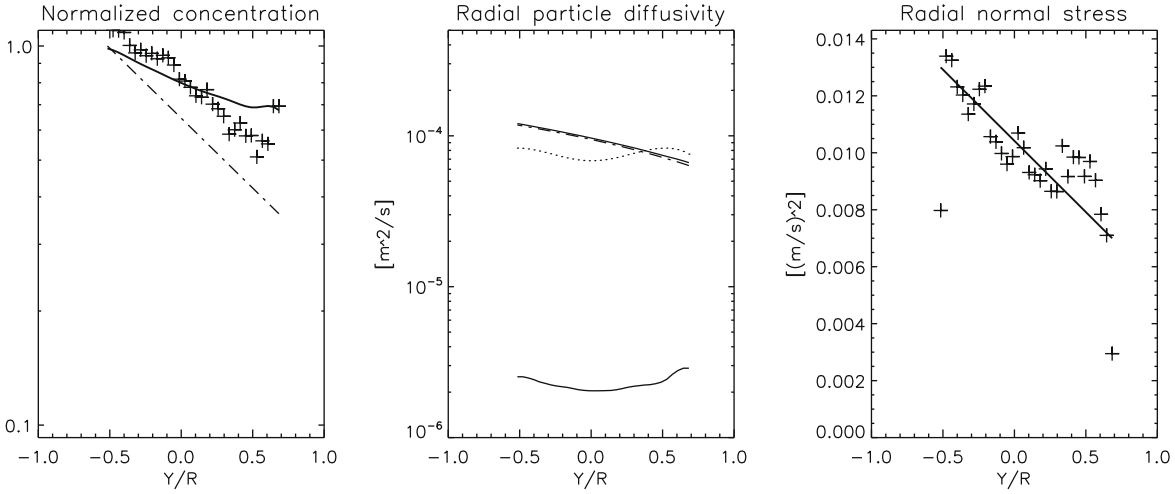

Fig. 14. Modelled concentration and radial diffusivity for Re = 115,000. The key is the same as in Fig. 12.

We conclude that (68) seems to be a sufficient governing equation for the concentration profiles (left panels), although some deviations are evident for the larger and smaller Reynolds numbers. The qualitative shape and curvature is captured, reflecting the variation of the particle diffusivity over the diameter and the presence of turbophoretic drift. It is worth noting that $\bar{\gamma}_y$ cancels the gradient of $\bar{\lambda}_{yy}$ within the PSA approximation. This simplifies the momentum equation considerably.

For all three Reynolds number cases, the normal kinetic stress is the dominating contributor to the diffusivity ($\tau_p\langle v'_y v'_y\rangle$ in the middle panels), and not the fluid diffusivity contribution $\tau_p\bar{\lambda}_{yy}$. We will see below that the source of kinetic stress is dominated by the added mass force, via the dispersion tensor component $\bar{\mu}_{yy}$.

5.2. Particle kinetic stress modeling

We will now calculate the normal stresses from the full stress equations (35) and (36), rather than using the data. Each equation is solved by using the measured stress of the other component – e.g., the wall normal stress equation is solved by using the linear fit to the measured axial stress as input. This approach is sufficient in order to test the validity of the governing equations. A fully self-contained solution can be obtained by solving these equations simultaneously.

The boundary conditions for the stress equations are taken as the endpoint values of the measured normal stress (also based on the linear fit). This choice has no large consequence, since the turbulent flux term (modelled by the Chapman–Enskog closure relation) is relatively small such that the stress equations are essentially local. The effects of boundary values are then not propagated very far into the domain (about 0.1 times the domain size).

The modelled concentration, diffusivity and normal stress profiles are shown in Figs. 15–17, where both local (thin full lines) and full solutions (thick line) of the stress are shown. The normal stresses (both radial and axial) are approximately given by local values governed by the algebraic relations (37) and (38) (the thin full line is almost indistinguishable from the thick full line). In order to obtain modeled stresses that are comparable to the measurements (thick full line, *lower left panels*), the particle interaction cross section is tuned to $d_h \simeq 6$ for all cases.

The slope of the normal stress profile in the lower half of the cross section (lower left panels) is controlled by the particle interaction contribution (dashed line), that transfer axial stress to radial stress. In the upper half of the cross section, the local stress source $\bar{\mu}_{yy}$ (dotted line) is larger than the stress redistribution term (for the two lower Reynolds numbers). The radial stress is therefore controlled by both particle interaction and the turbulent fluid forces. Furthermore, $\bar{\mu}_{yy}$ (lower left panels), is dominated by the

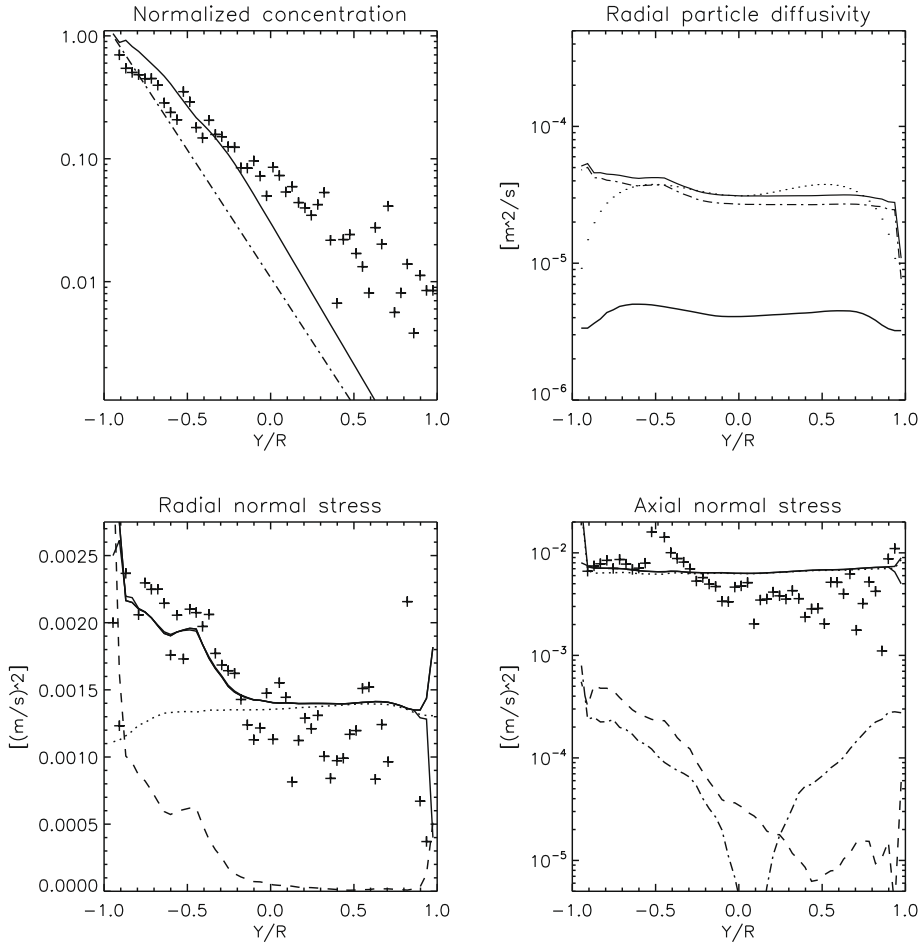

Fig. 15. Modelled normal stresses and concentration for $Re = 43{,}000$. (upper left panel) Crosses: data; thick line: model; straight dash-dotted line: exponential profile using the mean diffusivity. (upper right panel) Radial particle diffusivity; full thick line: ϵ_{yy}; dash-dotted thick line: $\tau_p\overline{v'_y v'_y}$ and dash-triple dotted line: $\tau_p\bar{\lambda}_{yy}$. The dotted line is the eddy viscosity. (lower left panel) Radial normal stress $\overline{v'_y v'_y}$. The crosses represent the data and the thick full line is the model prediction. The thin full line is the local stress given by (37), which is almost indistinguishable from the thick line. The dashed line shows the contribution due to particle–particle interaction. The dotted line is the contribution due to $\bar{\mu}_{yy}$. (Lower right panel) Axial normal stress $\overline{v'_x v'_x}$. The crosses represent the data and the thick full line is the model prediction. The thin full line is the local approximation (38), the dashed line is the contribution due to the particle–particle interaction. The dotted line is the contribution due to $\bar{\mu}_{xx}$ and the dash-dotted line is the shear induced contribution.

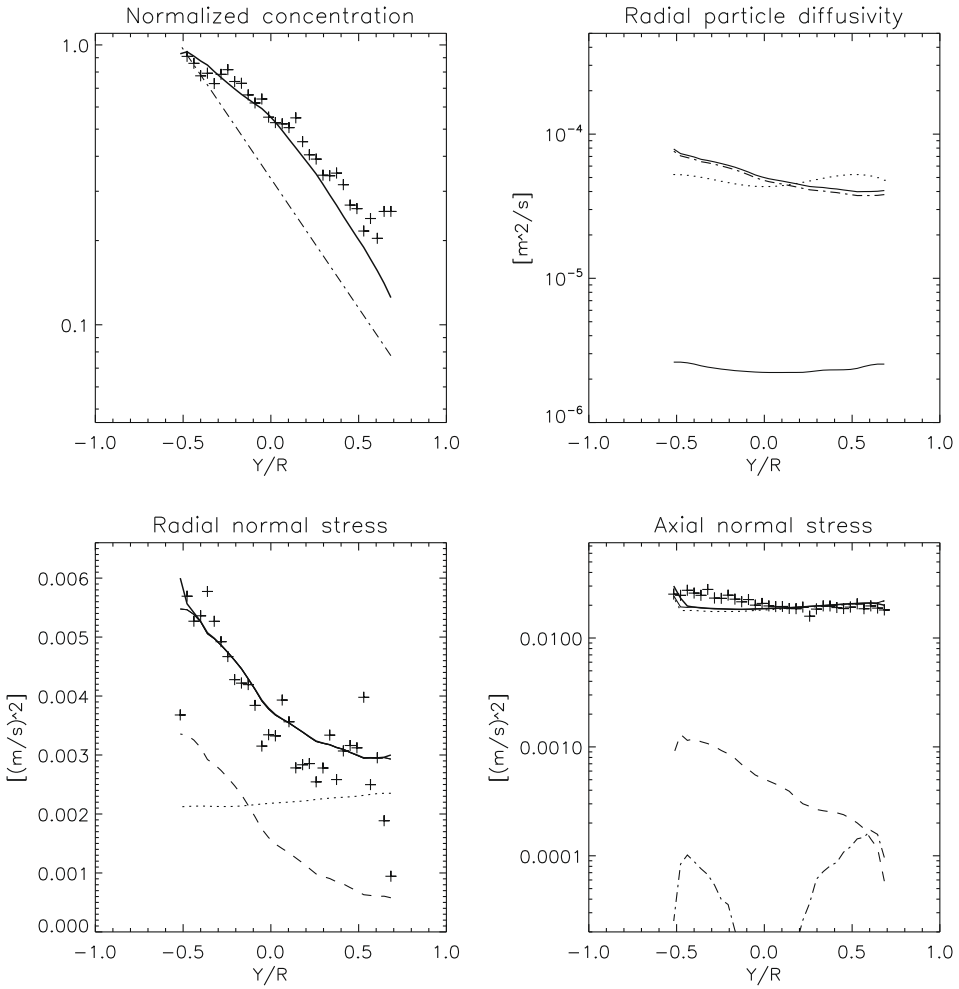

Fig. 16. Modelled normal stresses and concentration for Re = 63,900. The key is the same as in Fig. 15.

added mass contribution. Recall that this term accounts for the work done on the particles from all fluid forces.

The source for the axial stress $\bar{\mu}_{xx}$ (lower right panels) is also dominated by the added mass contribution.

Fig. 18 shows the axial stress for Re = 63,900 without the added mass forcing, and we conclude that the added mass effect is responsible for most of the axial stress. The two other Reynolds numbers show a similar dependency on the added mass force. Particle–particle interaction and mean shear provide negligible contributions to the axial stress (dashed and dash-dotted lines in the lower right panels in Figs. 15–17).

Fig. 19 shows the effect of ignoring particle–particle interaction. The modelled radial stress is now nearly constant since it is now independent of the particle concentration. The resulting diffusivity is also roughly constant for the same reason, and lower than what is needed to maintain a sufficient scale height for the concentration profile (upper left panel).

6. Discussion and conclusions

6.1. Interpretation of the data

6.1.1. Particle EOM

To test the validity of the EOM, we performed a cross-correlation between the particle acceleration $\dot{\mathbf{v}}$ and the adopted particle forces. We found a clear correlation between the particle acceleration $\dot{\mathbf{v}}$ and the fluid acceleration for the axial direction. Noise in the data prevented the same comparison to be made in the radial direction. For the axial direction, and for the current Reynolds numbers, we found that the fluid acceleration is more important in the particle EOM than the drag term, demonstrating the significant added mass forcing at the current particle/fluid material density ratio of 1.05.

6.1.2. Particle versus fluid stress

If we ignore stress transport and particle–particle interaction, the modelled radial normal stress of the particles is

$$\overline{v_y' v_y'} = \tau_p \bar{\mu}_{yy}.$$

With drag only, one can show that $\overline{v_y' v_y'} < \langle u_y' u_y' \rangle$, which is in contradiction to the data that show larger particle stress than fluid stress (Fig. 20). With added mass effects included in $\bar{\mu}_{yy}$, there is no such constraint. For symmetric fluid turbulence profiles in the cross section (ignoring turbulence modification), the particle stress profile will also be symmetric according to the local approximation of the dispersion tensor $\bar{\mu}_{yy}$. The measured radial stress shows, in contrast, a clear slope with larger stress near the pipe floor. This observation suggests that particle–particle hydrodynamic interactions are substantial enough to provide a clear concentration dependency.

6.1.3. Particle axial stresses

The axial stress is larger than the radial stress (Fig. 20, right panel), suggesting redistribution of axial stress to radial stress (collisions serve to make the stresses more isotropic). Furthermore, the

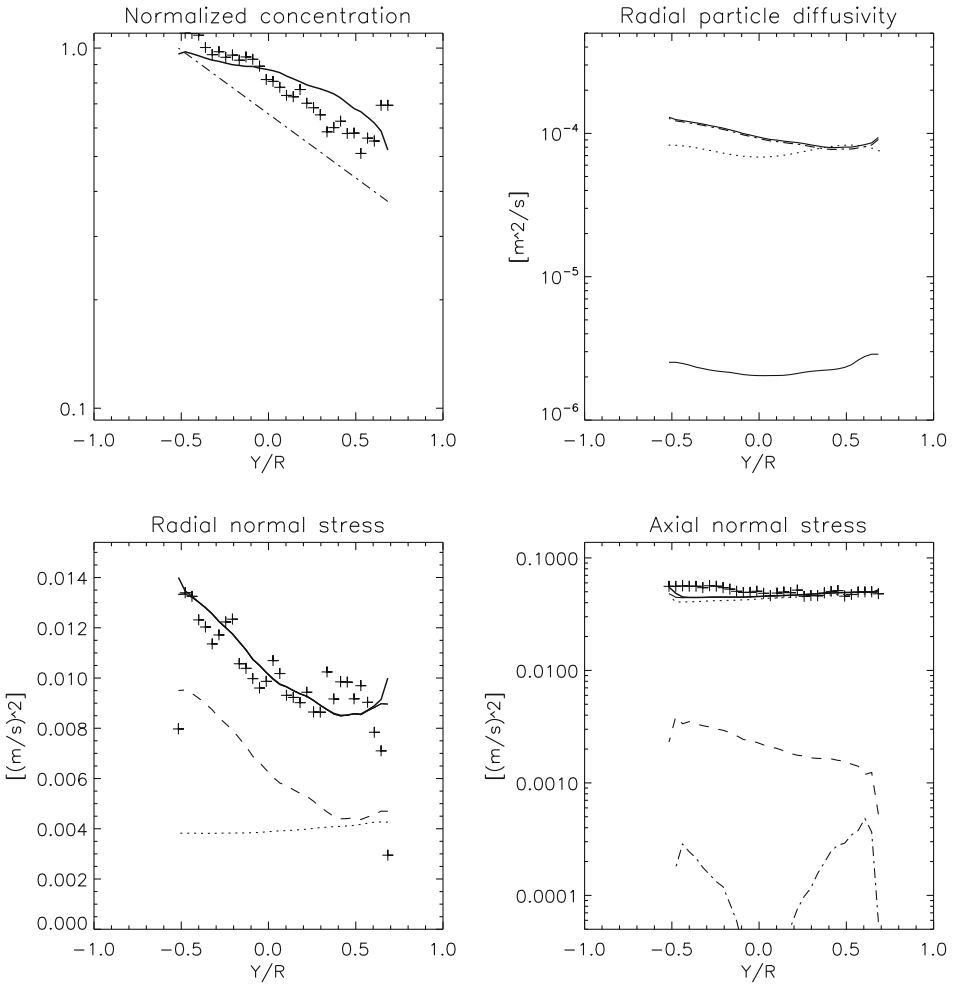

Fig. 17. Modelled normal stresses and concentration for Re = 115,000. The key is the same as in Fig. 15.

axial stress is more uniform than the radial stress, in terms of relative variation (compare the left and middle panels). This suggests that the axial stress is to a large degree generated by the local fluid–turbulence, providing a more uniform profile. We note here that stress redistribution is also observed in solids–gas flow (e.g., Caraman et al., 2003; Sommerfeld, 2003). Stress transport, wall interaction, and shear induced stress are also important ingredients in these flows, where the particle Stokes number is much larger than in the current setting.

6.2. Model results

To address the observations above, we have implemented a model based on the kinetic theory for a dilute suspension due to Reeks (1992). We modified the corresponding Eulerian stress equations by invoking the collision term of Simonin (2000), that serves to couple the stress tensor terms, with the effect of reducing the particle stress anisotropy. To account for long-range hydrodynamic interactions, we adopted an "effective cross section" of 6d, where d is the particle diameter. We solved the combined particle momentum and stress equations in channel flow geometry, to compare with the pipe flow data. The radial normal stress in the pipe is approximated by the wall normal stress from the channel flow model.

The wall normal particle diffusivity ϵ_{yy} controls to a large degree the local scale height ϵ_{yy}/V_T of the concentration profile (where V_T is the settling velocity corrected for buoyancy and added mass). It is found that the particle diffusivity is controlled by the kinetic stress (the fluid diffusivity contribution via $\bar{\lambda}$ plays only a minor role).

The gradient of particle kinetic stress generates a turbophoretic lift, which provides smaller corrections to the concentration profile. With added mass forcing, there is an additional wall normal lift due to the direct action of the gradient of turbulence pressure.

The wall normal kinetic stress that controls the diffusivity, is generated by a redistribution of axial stress by particle interaction (lower half of the flow volume), and by the added mass force (upper half of the flow volume) via $\bar{\mu}_{yy}$. The drag-force contribution to $\bar{\mu}_{yy}$ is less important. The source of axial stress is mainly due to the added mass contribution to $\bar{\mu}_{xx}$. The stress redistribution serves to suppress the axial stress, and shear generated axial stress is not important.

We found that a local approximation of the particle kinetic stress equations is sufficient, since the transport term can be ignored due to sufficiently small Stokes number (or characteristic diffusion length). Algebraic relations between the particle and fluid stresses, including the stress redistribution terms can then be invoked, eliminating the need for stress boundary conditions. Only for larger particle/fluid density ratios are stress boundary conditions necessary (such as droplets in gas modelled by Skartlien, 2009, or solid particles in gas).

Local stress relations, and the influence of added mass effects, give a wall normal diffusivity in the approximate local form

$$\epsilon_{yy} \simeq \tau_p(\overline{v_y' v_y'}) = \tau_p\left(\frac{\tau_p\bar{\mu}_{yy} + \frac{\tau_p}{\tau_c}\frac{\sigma_c}{3}q_p^2}{1-\frac{\tau_p}{\tau_c}\frac{\sigma_c}{2}}\right), \tag{69}$$

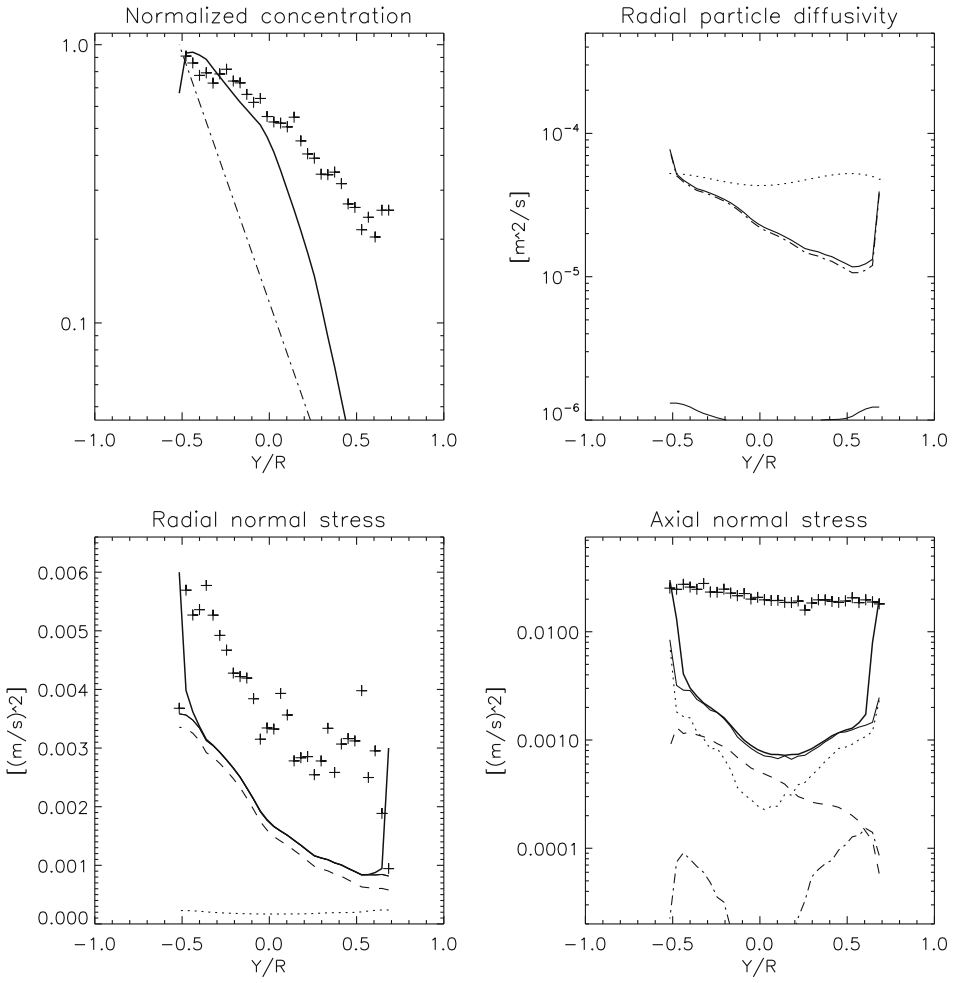

Fig. 18. Modelled normal stresses and concentration for Re = 63,900. No added mass effect. Only the drag-force and collisions are considered in this example. The axial stress, radial stress and radial diffusivity are underestimated. The radial stress does have the correct slope due to the particle interactions. The key is the same as in Fig. 15.

where

$$\bar{\mu}_{yy} \simeq \frac{\bar{\lambda}^{aa}_{yy}}{\tau_{aa}} = Q^{aa}_{yy}\frac{\tau_{aa}}{1+\beta\tau_{aa}-\alpha C''_{yy}\tau^2_{aa}}$$

is due to added mass forcing only, and the term in σ_c is due to the transfer of axial to radial kinetic stress.

6.3. Prospects

The current study has demonstrated the applicability of the kinetic theory also in cases where (1) the added mass forcing due to fluid acceleration is important and (2) in "semi-dense" suspensions where hydrodynamic interactions are significant. To obtain a fully self contained model, we would require a separate model for the acceleration correlation tensors, and the associated correlation times. This can possibly be achieved by applying the Pope (2002) approach for the acceleration correlations using the Langevin approach. The model may also be applied to flows where the added mass term completely dominates, such as bubble flow or for emulsion droplets.

Acknowledgement

This project was funded by the Research Council of Norway via "Strategic Institute Project ES132014, Droplet Transport Modeling and Generation Enhancement in Hydrocarbon Multiphase Transport". Sven Nuland and John Grue initiated the project. We would like to acknowledge cooperation with the Norwegian "Flow Assurance Center" (FACE) via the participation of D.C. Swailes. It is a pleasure to acknowledge M.W. Reeks and P. van Dijk at the University of Newcastle, UK, for invaluable input and Chris Lawrence, IFE, for suggestions on improving the manuscript.

Appendix A. Diffusion equation for the particles

The mass flux density is expressed by recasting the momentum equation (19) in the diffusion equation form

$$\rho\overline{v_i} = -\epsilon_{ik}\partial_k\rho - \rho\tau_p\left(\bar{\gamma}_i - \overline{F}_i\right) - \rho\tau_p\partial_k\left(\overline{v'_i v'_k} + \bar{\lambda}_{ki}\right) - \tau_p\rho\frac{D\overline{v_i}}{Dt}, \qquad (A.1)$$

where $\tau_p\partial_k(\overline{v'_i v'_k})$ is the turbophoretic drift velocity in the i-direction, $D/Dt = \partial_t + \overline{v_k}\partial_k\overline{v_i}$, and the diffusivity tensor ϵ_{ik} enters naturally as a gradient diffusion coefficient. For zero mean velocity, this equation alone governs the density distribution of the particles via a first order equation with variable coefficients, when the kinetic stress and the dispersion tensors are given.

Appendix B. Force correlation functions in local form

B.1. Drag contribution

The two-point drag-force correlation is

$$\langle d_i d_k\rangle = \beta^2\langle u'_i u'_k\rangle. \qquad (B.1)$$

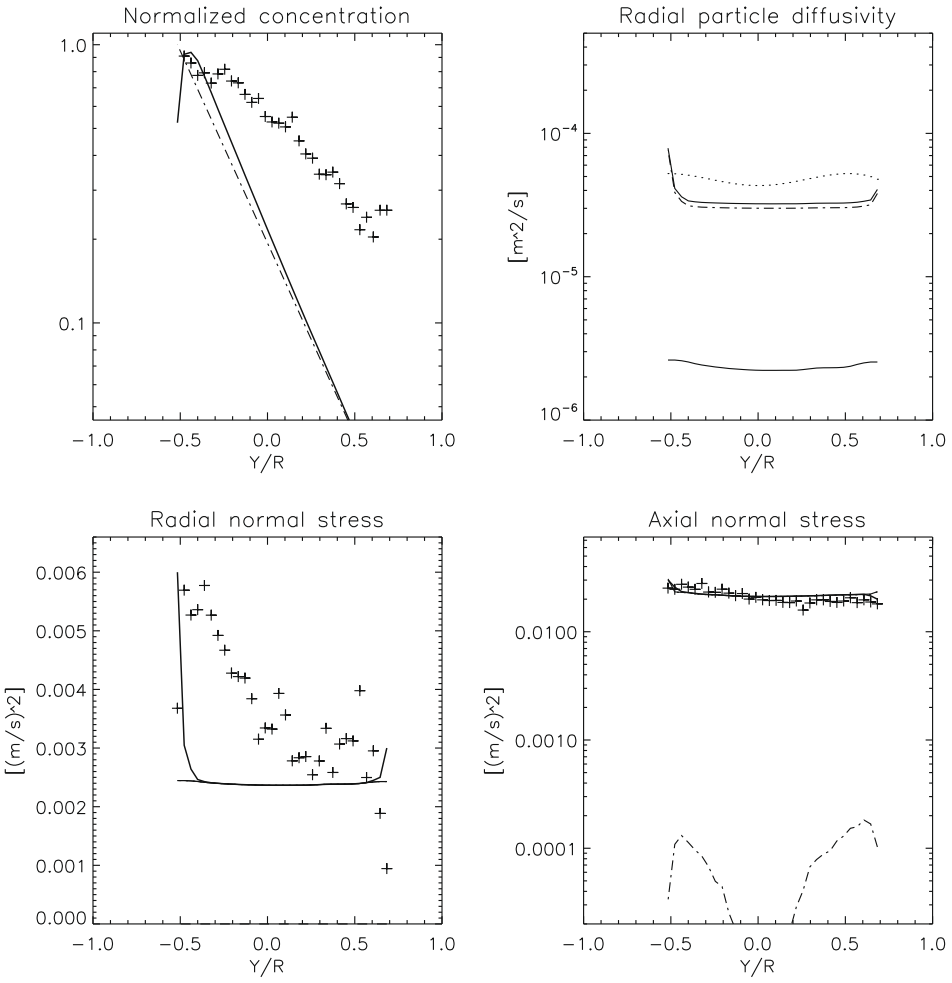

Fig. 19. Modelled normal stresses and concentration for $Re = 63{,}900$. No collisions. Only the drag-force and added mass is considered in this example. The radial stress is underestimated and symmetric due to the absence of particle interaction. The resulting diffusivity is also roughly symmetric for the same reason. The key is the same as in Fig. 15.

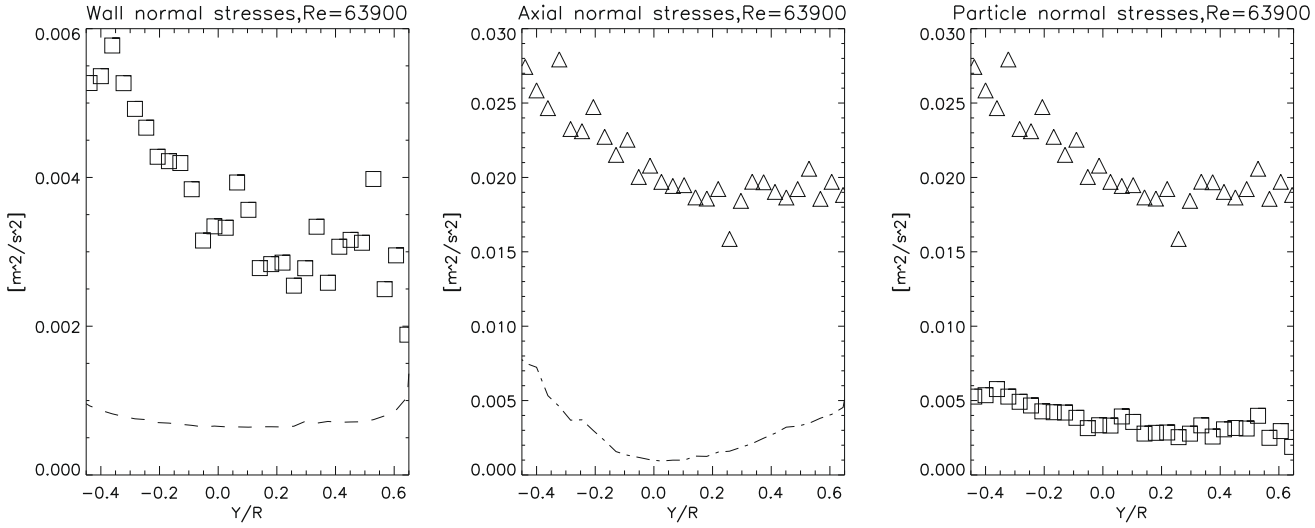

Fig. 20. Measured fluid and particle normal stresses for $Re = 63{,}900$. Symbols represent the particle stresses and lines the fluid stresses. The left panel shows the radial stresses and the middle panel the axial stresses. The particle stresses are larger than the fluid stresses due to added mass forcing (fluid acceleration). The radial and axial particle stress are compared in the right panel. The axial particle stress is larger than the radial particle stress and the model shows that axial stress is transferred to radial stress via hydrodynamic particle–particle interaction.

The local approximation assumes the following form:

$$R_{ik}^{dd} = \langle d_i d_k \rangle = \beta^2 \langle u_i'(\mathbf{x}) u_k'(\mathbf{x}) \rangle e^{-(t-s)/\tau}, \tag{B.2}$$

where τ is the correlation time of the turbulent velocity fluctuations as measured along the particle paths, and $\beta^2 \langle u_i'(\mathbf{x}) u_k'(\mathbf{x}) \rangle = Q_{ik}^{dd}$ is the local single-point correlation. It is assumed that the same correlation time applies to all combinations of velocity components.

B.2. Combined drag – added mass contribution

From the Navier–Stokes equation, we obtain the fluctuating fluid acceleration

$$\left(\frac{D\mathbf{u}}{Dt}\right)_i' = \left(\frac{D\mathbf{u}}{Dt}\right)_i - \overline{\left(\frac{D\mathbf{u}}{Dt}\right)_i} = \tag{B.3}$$

$$\partial_t u_i' + u_j \partial_j u_i' + u_j' \partial_j \bar{u}_i - \partial_j \overline{u_i' u_j'} = \tag{B.4}$$

$$f_i'/\rho - \partial_i p'/\rho + \nu \nabla^2 u_i'. \tag{B.5}$$

In statistically stationary flow, the cross terms (44) become

$$\langle d_i a_k \rangle + \langle a_i d_k \rangle = \alpha\beta \left\langle u_k' \left(\frac{D\mathbf{u}}{Dt}\right)_i' + u_i' \left(\frac{D\mathbf{u}}{Dt}\right)_k' \right\rangle = \alpha\beta \left\langle u_k' \frac{Du_i'}{Dt} + u_i' \frac{Du_k'}{Dt} \right\rangle + \alpha\beta \langle u_k' u_j' \partial_j \bar{u}_i \rangle + \alpha\beta \langle u_i' u_l' \partial_l \bar{u}_k \rangle + \alpha\beta A, \tag{B.6}$$

where (ignoring $\langle u_i' \partial_t u_k' + u_i' \partial_t u_k' \rangle$)

$$\left\langle u_k' \frac{Du_i'}{Dt} + u_i' \frac{Du_k'}{Dt} \right\rangle = \bar{u}_j \langle u_k' \partial_j u_i' + u_i' \partial_j u_k' \rangle + \langle u_i' u_j' \partial_j u_k' + u_k' u_j' \partial_j u_i' \rangle + \langle u_i' [u_j(\mathbf{x}_p) - u_j(\mathbf{x})] \partial_j u_k' \rangle, \tag{B.7}$$

$$A = \langle u_k' \partial_j \overline{u_j' u_i'} \rangle + \langle u_i' \partial_l \overline{u_l' u_k'} \rangle. \tag{B.8}$$

We note that for $s = t$, we recover terms in the standard (single point) Reynolds stress equation. That is, for $\mathbf{x}_p = \mathbf{x}$,

$$\left\langle u_k' \left(\frac{D\mathbf{u}}{Dt}\right)_i' + u_i' \left(\frac{D\mathbf{u}}{Dt}\right)_k' \right\rangle = \bar{u}_j \partial_j \langle u_i' u_k' \rangle + \partial_j \langle u_j' u_i' u_k' \rangle + \langle u_k' u_j' \rangle \partial_j \bar{u}_i + \langle u_i' u_j' \rangle \partial_j \bar{u}_k, \tag{B.9}$$

where the angle brackets for ensemble averaging over particle positions reduce to local ensemble averages, which again can be replaced by time averages. The remaining terms vanish since the average fluctuation is zero (therefore $A = 0$) and $[u_j(\mathbf{x}_p) - u_j(\mathbf{x})] = 0$.

We make the following hypothesis to conform to local homogeneity: The two-point correlations in (B.6) can be expressed in terms of a time dependent exponential decay of the local single-point correlations in the local form (B.9). For strictly homogeneous turbulence, the single-point advection and flux divergence in (B.9) vanish. Only the production term remains, and we adopt the following local approximation:

$$\langle d_i a_k \rangle + \langle a_i d_k \rangle = \alpha\beta \left(\langle u_k' u_j' \rangle \partial_j \bar{u}_i + \langle u_i' u_j' \rangle \partial_j \bar{u}_k \right) e^{-(t-s)/\tau_{ad}}, \tag{B.10}$$

where τ_{ad} is a suitable correlation time of the two-point correlation function between the added mass force and the drag-force.

In the case of homogeneous turbulence with shear due to a mean velocity in the x-direction, the components read

$$\begin{aligned} \langle d_x a_x \rangle + \langle a_x d_x \rangle &= 2\alpha\beta \left(\langle u_x' u_y' \rangle \partial_y \bar{u}_x \right) e^{-(t-s)/\tau_{ad}}, \\ \langle d_x a_y \rangle + \langle a_x d_y \rangle &= \alpha\beta \left(\langle u_y' u_y' \rangle \partial_y \bar{u}_x \right) e^{-(t-s)/\tau_{ad}}, \\ \langle d_y a_y \rangle + \langle a_y d_y \rangle &= 0. \end{aligned} \tag{B.11}$$

For components involving the spanwise direction z,

$$\begin{aligned} \langle d_x a_z \rangle + \langle a_x d_z \rangle &= \alpha\beta \left(\langle u_z' u_y' \rangle \partial_y \bar{u}_x \right) e^{-(t-s)/\tau_{ad}}, \\ \langle d_y a_z \rangle + \langle a_y d_z \rangle &= 0, \\ \langle d_z a_z \rangle + \langle a_z d_z \rangle &= 0. \end{aligned} \tag{B.12}$$

B.3. Added mass contribution

The two-point (non-local) correlation function of the added mass force can be written

$$\langle a_i a_k \rangle \simeq \alpha^2 \left(\langle \partial_t u_i' \partial_t u_k' \rangle + \langle \partial_j (u_j u_i)' \partial_l (u_l u_k)' \rangle \right), \tag{B.13}$$

where $(u_j u_i)' = u_j u_i - \overline{u_j u_i}$ is the stress fluctuation in the fluid. For the diagonal elements $i = k$ and for $j = l$, the correlation is clearly positive. We may adopt an order of magnitude estimate directly,

$$\langle a_i a_k \rangle \sim \alpha^2 \frac{\langle u_i' u_k' \rangle}{\hat{\tau}_i \hat{\tau}_k} e^{-(t-s)/\tau_{aa}}, \tag{B.14}$$

where $\hat{\tau}_i$ is a characteristic time for the fluid acceleration Du_i/Dt.

Appendix C. Green's function for the EOM

The displacement Greens function is needed to calculate the dispersion tensors. The particle displacement in the i direction due to an impulsive force applied in the j direction is, in the presence of a mean force and a simple drag coefficient without lift, given by the solution of the system of equations (e.g., Hyland et al., 1999)

$$\ddot{G}_{ji} + \beta \dot{G}_{ji} - G_{jk} \partial_k F_i = \delta_{ij} \delta(t - s), \tag{C.1}$$

where δ_{ij} is the Kronecker delta. In channel flow, the mean force varies only in y, such that $G_{jk} \partial_k F_i = G_{jy} \partial_y F_i$. For the force gradients, we get

$$\partial_y F_x = \beta \partial_y \langle u_x \rangle + \alpha \partial_y^2 \langle u_x' u_y' \rangle \equiv \beta S + \alpha C_{xy}'' = B_1, \tag{C.2}$$

$$\partial_y F_y = \alpha \partial_y^2 \langle u_y' u_y' \rangle \equiv \alpha C_{yy}'' = B_2. \tag{C.3}$$

The initial conditions are

$$G_{ij}(0) = 0, \tag{C.4}$$

$$\dot{G}_{ij}(0) = \delta_{ij}, \tag{C.5}$$

where $\dot{G}_{ij} = \partial_t G_{ij}$. These conditions follow from the Dirac delta function forcing of the diagonal elements G_{ii}. The first conditions simply states zero displacement at time zero. The resulting Greens function components (that are needed here) are

$$G_{xx} = \beta^{-1}(1 - e^{-\beta t}), \tag{C.6}$$

$$G_{yy} = (\Delta\beta)^{-1}(e^{m_2 t} - e^{m_1 t}), \tag{C.7}$$

$$G_{yx} = \frac{B_1}{\beta \Delta B_2} \left[(e^{m_2 t} - e^{m_1 t}) - \Delta(1 - e^{-\beta t}) \right], \tag{C.8}$$

$$G_{xy} = 0, \tag{C.9}$$

where

$$m_1 = -\frac{\beta}{2}(1 + \Delta), \tag{C.10}$$

$$m_2 = -\frac{\beta}{2}(1 - \Delta), \tag{C.11}$$

$$\Delta = \sqrt{1 + \eta^2 C_{yy}''}, \tag{C.12}$$

$$\eta = \frac{4\alpha}{\beta}. \tag{C.13}$$

The G_{yx} component expresses the streamwise particle displacement due to a force in the vertical direction (due to the mean shear). Both G_{yx} and G_{yy} are influenced by the added mass contribution to the mean force (via Δ and the Reynolds stress gradients).

Appendix D. Calculation of the dispersion tensors

The two forces (added mass and drag), give three contributions to each of the three dispersion tensor components. In general,

$$\bar{\lambda}_{ji}(y) = \sum_m \sum_n \int_{-\infty}^{0} R_{ik}^{mn}(y,t,s) G_{kj}(t-s) ds = (\bar{\lambda}_{ji})_{dd} + (\bar{\lambda}_{ji})_{ad} + (\bar{\lambda}_{ji})_{aa}. \quad \text{(D.1)}$$

By invoking the local form (47), one obtains

$$\bar{\mu}_{ji}(y) = \sum_m \sum_n \int_{-\infty}^{0} R_{ik}^{mn}(y,t,s) \dot{G}_{kj}(t-s) ds = \frac{(\bar{\lambda}_{ji})_{dd}}{\tau} + \frac{(\bar{\lambda}_{ji})_{ad}}{\tau_{ad}} + \frac{(\bar{\lambda}_{ji})_{aa}}{\tau_{aa}}. \quad \text{(D.2)}$$

Green's function G_{kj} for the EOM is given in Appendix C. The two drag-added mass contributions (*ad* and *da*) are merged into one dispersion tensor.

For the dispersion vector component $\bar{\gamma}_y$, we adopt the passive scalar approximation – PSA (Skartlien, 2007),

$$\bar{\gamma}_y = -\partial_y(\bar{\lambda}_{yy}). \quad \text{(D.3)}$$

This approximation assures the correct behavior for the momentum equation in incompressible flow in the limit of small particle Stokes number. We can take $\bar{\gamma}_x = \bar{\gamma}_z = 0$ since the turbulence inhomogeneity is only felt in the *y*-direction, perpendicular to the channel walls.

References

Ahmed, A.M., Elghobashi, S.E., 2000. On the mechanism of modifying the structure of turbulent homogeneous shear flows by dispersed particles. Phys. Fluids 12, 2906–2930.

Auton, T.R., Hunt, J.C.R., Prud'homme, M., 1988. Force exerted on a body in inviscid unsteady non-uniform rotational flow. J. Fluid Mech. 197, 241–257.

Batchelor, G.K., 1967. An Introduction to Fluid Dynamics. Cambridge University Press, Cambridge.

Caraman, N., Borée, J., Simonin, O., 2003. Effect of collisions on the dispersed phase fluctuation in a dilute tube flow: experimental and theoretical analysis. Phys. Fluids 15, 3602–3612.

Crowe, C.T., 2000. On models for turbulence modulation in fluid–particle flows. Int. J. Multiphase Flow 26, 719–727.

Drazen, D., Jensen A., 2007. Time-resolved combined PIV/PTV measurements of two-phase turbulent pipe flow. In: Proceeding of the 6th International Conference on Multiphase Flow, ICMF 2007, Leipzig, Germany, July 9–13, 2007.

Drazen, D., Jensen A., in preparation. Lagrangian measurements of two-phase pipe flow using combined PIV/PTV.

Elghobashi, S.E., Abou-Arab, T.W., 1983. A two-equation model for two-phase flows. Phys. Fluids 26, 931–938.

Ferrante, A., Elghobashi, S.E., 2003. On the physical mechanisms of two-way coupling in particle-laden istotropic turbulence. Phys. Fluids 15, 315–329.

Gore, R.A., Crowe, C.T., 1989. Effect of particle size on modulating turbulent intensity. Int. J. Multiphase Flow 15, 279–285.

Grad, H., 1949. On the kinetic theory of rarefied gases. Commun. Pure Appl. Math. 2, 331–407.

Hetsroni, G., 1989. Particles–turbulence interaction, Int. J. Multiphase Flow 15, 735–746.

Hyland, K.E., McKee, S., Reeks, M.W., 1999. Derivation of a pdf kinetic equation for the transport of particles in turbulent flows. J. Phys. A: Math. Gen. 32, 6169–6190.

Jenkins, J.T., Richmann, M.W., 1985. Grad's 13-moment system for a dense gas of inelastic spheres. Arch. Ration. Mech. Anal. 87, 355–377.

Jensen, A., Pedersen, G.K., 2004. Optimization of acceleration measurements using PIV. Meas. Sci. Technol. 15, 2275–2283.

Johnson, T.A., Patel, V.C., 1999. Flow past a sphere up to a Reynolds number of 300. J. Fluid Mech. 378, 19–70.

Kataoka, I., Serizawa, A., 1989. Basic equations of turbulence in gas–liquid two-phase flow. Int. J. Multiphase Flow 15, 843–855.

Kenning, V.M., Crowe, C.T., 1997. On the effect of particles on carrier phase turbulence in gas–particle flows. Int. J. Multiphase Flow 23, 403–408.

Kiger, K.T., Pan, C., 2000. PIV technique for the simultaneous measurement of dilute two-phase flows. J. Fluids Eng. 122, 811–818.

Lightstone, M.F., Hodgson, S.M., 2004. Turbulence modulation in gas–particle flows: a comparison of selected models. Can. J. Chem. Eng. 82, 209–219.

Maxey, M.R., Riley, J.J., 1983. Equation of motion for a small rigid sphere in a non-uniform flow. Phys. Fluids 26, 883–889.

Pope, S.B., 2002. A stochastic Lagrangian model for acceleration in turbulent flows. Phys. Fluids 14, 2360–2375.

Poelma, C., Ooms, G., 2006. Particle–turbulence interaction in a homogeneous, isotropic turbulent suspension. Trans. ASME 59, 78–90.

Reeks, M.W., 1992. On the continuum equations for dispersed particles in nonuniform flows. Phys. Fluids A 4, 1290–1303.

Reeks, M.W., 1993. On the constitutive relations for dispersed particles in nonuniform flows. 1: Dispersion in a simple shear flow. Phys. Fluids A 5, 750–761.

Reeks, M.W., 2005. On model equations for particle dispersion in inhomogeneous turbulence. Int. J. Multiphase Flow 31, 93–114.

Sergeev, Y.A., Johnson, R.S., Swailes, D.C., 2002. Dilute suspension of high inertia particles in the turbulent flow near the wall. Phys. Fluids 14, 1042–1055.

Sommerfeld, M., 2003. Analysis of collision effects for turbulent gas–particle flow in a horizontal channel: Part1: Particle transport. Int. J. Multiphase Flow 29, 675–699.

Simonin, 2000. Statistical and continuum modelling of turbulent reactive particulate flows – Lecture Notes Part 1.

Skartlien, R., 2007. Kinetic modeling of particles in stratified flow – evaluation of dispersion tensors in inhomogeneous turbulence. Int. J. Multiphase Flow 33, 1006–1022.

Skartlien, R., 2007b. Evaluation of a kinetic theory model for inertial particles in stratified turbulent flow – the influence of the Stokes number. In: Proceedings of the 6th International Conference on Multiphase Flow, ICMF 2007, Leipzig, Germany, July 9–13, 2007.

Skartlien, R., 2009. A droplet transport model for channel and pipe flow based on particle kinetic theory and a stress–ω turbulence model. Int. J. Multiphase Flow 35, 603–616.

Swailes, D.C., Sergeev, Y.A., Parker, A., 1998. Chapman–Enskog closure approximation in the kinetic theory of dilute turbulent gas–particulate suspensions. Physica A 254, 517–547.

Wang, Y., Komori, S., Chung, K.K., 1997. A two-fluid turbulence model for gas–solid two-phase flows. J. Chem. Eng. Jpn. 30, 3, 526–53.

Wu, Y., Wang, H., Liu, Z., Li, J., Zhang, L., Zheng, C., 2006. Experimental investigation on turbulence modification in horizontal channel flow at relatively low mass loading. Acta Mech. Sinica 22, 99–108.

Young, J., Leeming, A., 1997. A theory of particle deposition in turbulent pipe flow. J. Fluid Mech. 340, 129–159.

Zaichik, L.I., Alipchenkov, V.M., 2005. Statistical models for predicting particle dispersion and preferential concentration in turbulent flows. Int. J. Heat Fluid Flow 26, 416–430.